Macrophages stimulate epicardial VEGFaa to trigger cardiomyocyte proliferation in larval zebrafish heart regeneration

Finnius A. Bruton[1]* , Aryan Kaveh[1], Katherine Ross-Stewart[1], Gianfranco Matrone[1], Magdalena Oremek[2], Emmanouil G. Solomonidis[1], Carl Tucker[1], John Mullins[1], Mairi Brittan[1], Jonathan Taylor[3], Adriano Rossi[2], Martin Denvir[1].

[1]Centre for Cardiovascular Science, Queen's Medical Research Institute, University of Edinburgh, Edinburgh, United Kingdom.

[2]Centre for Inflammation Research, Queen's Medical Research Institute, University of Edinburgh, Edinburgh, United Kingdom.

[3]Department of Physics, University of Glasgow, Glasgow, United Kingdom.

Corresponding author: *

Abstract

Cardiac injury induces a sustained innate immune response in both zebrafish and mammals. Macrophages, highly plastic immune cells, perform a range of both beneficial and detrimental functions during mammalian cardiac repair yet their precise roles in zebrafish cardiac regeneration are not fully understood. Here we characterise cardiac regeneration in the rapidly regenerating larval zebrafish laser injury model and use macrophage ablation and macrophage-less *irf8* mutants to define the requirement of macrophages for key stages of regeneration. We found macrophages to display cellular heterogeneity and plasticity in larval heart injury as in mammals. Live heartbeat-synchronised imaging and RNAseq revealed an early proinflammatory macrophage phase which then resolves to an anti-inflammatory, profibrotic phase. Macrophages are required for cardiomyocyte proliferation but not for functional or structural recovery following injury. Macrophages are specifically recruited to the epicardial-myocardial niche, triggering the expansion of the epicardium which upregulates mitogen VEGFaa. Experimental perturbation of VEGF signalling confirmed VEGFaa to be an important inducer of cardiomyocyte proliferation revealing

a previously unrecognised mechanism by which macrophages aid cardiac regeneration.

Introduction

Zebrafish are highly regenerative, exhibiting the capacity to restore full structure and functionality of a wide range of different tissues following injury or degeneration[1–5]. Cardiac injury is one such example where adult mammals are only able to facilitate maladaptive repair whilst zebrafish exhibit full tissue regeneration[6,7]. In humans, the most clinically severe form of cardiac injury is myocardial infarction (MI), where occlusion of a coronary artery triggers ischemic injury to the myocardium leading to the loss of approximately 1 billion cardiomyocytes[8]. Adult mammalian cardiomyocytes are considered post-mitotic, switching to hypertrophic growth shortly after birth and are therefore unable to restore lost myocardium which is instead replaced with non-contractile scar tissue[9]. MI patients suffer a sequel of maladaptive remodelling leading to left ventricular dilation and thinning of the scar further decreasing the function of the heart[10,11]. Therefore, there is a need for medical innovation which can reverse this process.

In contrast to mammals, apical resection and cryoinjury models of MI in zebrafish show full regeneration of lost myocardium via the dedifferentiation and proliferation of surviving cardiomyocytes[12,13]. Cardiac regeneration is complex and dynamic, with zebrafish hearts undergoing debridement of dead myocardium, followed by transient fibrosis, revascularisation and subsequent replacement of cardiomyocytes[14]. The inflammatory response has been demonstrated to be crucial for each of these key events, both in zebrafish and also other regenerative species such as axolotls and neonatal mice[15–17]. Innate immune cells ‘macrophages’ have emerged as important regulators of tissue regeneration. Indeed macrophage ablation has been shown to abrogate regeneration across multiple organs and organisms, including the zebrafish heart[15,16,18–22].

However, the precise contribution of macrophages to cardiac repair has been complicated by disparate results following macrophage perturbation in murine models of MI[7,23–25]. This is in part attributed to substantial heterogeneity of macrophage

subtypes and individual phenotypic plasticity[26,27]. Incidentally it is these same qualities that make macrophages ideally suited to modulating the dynamic signalling and cellular patterning of cardiac regeneration. Hence, macrophages are understood to exist on a multidimensional spectrum of phenotypes, informed both by the interaction environmental stimuli and ontological memory[28]. Recent studies have confirmed the presence of macrophage subsets in zebrafish yet their functional niche and interactions with other key cell types of the heart, such as the epicardium, remain poorly understood[29,30].

Larval zebrafish regenerate more rapidly than adults, occurring in just 48 hours after cardiac laser injury in 3-day old larvae[31,32]. Combined with their amenability for live *in vivo* imaging and genetic tractability, this model becomes a powerful tool with which to carefully examine how macrophages support multiple aspects of cardiac regeneration.

Here we perform an in-depth characterisation of several key processes in larval zebrafish cardiac regeneration, finding the heart regeneration program between the larvae and adult to be highly conserved. Perturbation of macrophage presence following injury using metronidazole-nitroreductase ablation or the macrophage null *irf8-/-* mutant[33] demonstrated a requirement for these cells in removal of apoptotic cells, epicardial activation and cardiomyocyte proliferation. We found that epicardial VEGFaa is required to induce cardiomyocyte proliferation following injury. Macrophages invade the epicardial-myocardial niche and ablation of macrophages prior to injury blocks epicardial expansion, preventing an increase of VEGFaa expression and therefore precluding cardiomyocyte proliferation.

Results

Macrophages display cellular heterogeneity following cardiac injury

We have previously demonstrated a sustained macrophage response to cardiac injury in zebrafish larvae[32] but it is not yet known if these cells are heterogenous and contain subsets. Thus the heterogeneity of macrophages following tissue injury is limited to a

handful of studies where fluorescent reporter lines have been combined to visualise subsets[18,29,30,34]. To assess macrophage heterogeneity following cardiac injury, we crossed the widely used zebrafish pan macrophage reporter line *Tg(mpeg1:GFP)* with *Tg(csf1ra:gal4;UAS:mCherry-NfsB)* (shortened here to csf1ra: mCherry). csf1ra (colony stimulated factor 1 receptor) is a cytokine required for macrophage development and used as a macrophage reporter promotor in mammals.

Larval hearts were lasered at the ventricular apex at 72 hours post-fertilisation (hpf) and subsequently imaged at 2, 6, 24, and 48 hours post injury (hpi) timepoints (Figure 1a). Macrophages migrate to the injured ventricular apex within two hours, peak at 6 and maintain elevated numbers until 48 hpi (Figures 1b & 1c). We found not all recruited macrophages were co-positive for both transgenes, leading to three subsets 1) mpeg1+csf1ra- (19.3±5.1%), 2) mpeg1-csf1ra+ (2.8±2.1%) and 3) mpeg1+csf1ra+ (77.9±5.7%). Similar dynamics were seen for subsets 1 & 3 but since mpeg1-csf1ra+ were exceedingly rare (most often not present at all in injured hearts) it is not possible to know if the dynamics are likewise similar. Both subsets exhibit a range of morphologies with no overt difference (Figure 1d, Video 1). Whole-larva epifluorescence images revealed an anterior-posterior gradient of co-positivity, with most macrophages being mpeg1+csf1ra+ anteriorly and decreasing *csf1ra*:mCherry positivity toward the tail (Supplementary Figure 1a). Taken together, our data demonstrate that larval macrophages recruited to cardiac injury are heterogenous in their markers, similar to adult zebrafish and mouse models[23,34].

Macrophages display cellular plasticity following cardiac injury

Macrophages also display remarkable plasticity in their phenotypes, changing activation states via enhancer landscapes in response to extrinsic stimuli[27]. In zebrafish, *tnfα* has emerged as a convenient marker for inflammatory macrophages, with several studies reporting their importance for a tissue regeneration in a variety of tissues[18,21,30].

We therefore performed cardiac laser injury on *Tg(tnfα:GFP;mpeg1:mCherry)* larvae, finding a subset of mpeg1+ macrophages to be marked by *tnfα*:GFP expression

(Figure 1e). Quantification of tnfα+ macrophage number revealed this subset is transient, found only at the 24 hpi timepoint and rarely in uninjured larvae (Figure 1g). At the 24 hpi, tnfα+mpeg1+ macrophages make up just 19.3±4.9% of macrophages whereas the majority (71.8±6.2%) are tnfα-mpeg1+ (Supplementary figure 1b). Surprisingly, the remaining 8.8±4.1% of injury-recruited cells are tnfα+mpeg1-, displaying macrophage morphology and behaviour.

We reasoned that if these tnfα+ macrophages were indeed inflammatory macrophages then it should be possible to increase their abundance via application of M1-polarisation cytokine IFN-γ. A single intravenous injection of zebrafish recombinant protein IFN-γ-rel immediately prior to cardiac injury increased the proportion of tnfα+mpeg1+ macrophages from 26.4±11.0% in PBS injected controls to 78.8±9.5%, supporting the idea that these are inflammatory macrophages (Supplementary figure 1c-e).

To verify whether this is plasticity at the level of individual cells or recruitment of a pre-polarised subtype, we performed *in vivo* imaging live in the beating heart. Timelapse imaging clearly showed recruited macrophages becoming tnfα:GFP+ after arrival at the injured ventricle, confirming that this represents an *in situ* conversion (Figure 1g, Supplementary video 2). Conversely, we also observed an instance of a tnfα+mpeg1+ arriving at the injured ventricle pre-converted (Figure 1g). Finally, we observed that macrophages appear to retract pseudopods and become spherical once arriving at the ventricle (Supplementary figure 1f).

Metronidazole-nitroreductase ablation and *irf8*-/- mutants provide a macrophage null injury setting

We next sought to understand what role macrophages are playing in the regeneration of the larval heart, which occurs after just 48 hours[31,32]. To test this, we used two completely different methods to induce macrophage-less hearts. Firstly we used the *Tg(csf1ra:gal4;UAS:mCherry-nfsB)* line that expresses a nitroreductase enzyme 'nfsB' in macrophages, leading to cell-specific apoptosis when exposed to prodrug

metronidazole[35]. We were able find dose that ablated macrophages but left other cells such as neutrophils unaffected (Figure 2b & 2c, Supplementary figure 2a-d) and able to respond to wounds (Supplementary figure 2e). We were able completely abolish macrophage recruitment, with only mpeg1+/csf1ra+ cells being 1-2 apoptotic bodies of resident cardiac macrophages (Figure 2a & 2d).

The second method was the use of the macrophage null *irf8*-/- mutant. This mutant lacks the expression of irf8, a transcription factor required for macrophage development. This mutation generates macrophage null animals which are otherwise phenotypically normal (Figure 2e, Supplementary figure 3a-e)[33]. Presence of the mutation was verified both the presence of the mutation by PCR (Figure 2f) and the absence of macrophages by vital stain neutral red (Figure 2g). Both models therefore provide powerful tools to dissect the role of macrophages in heart regeneration in larval zebrafish.

Macrophages contribute to the removal of apoptotic cardiomyocytes following injury

The best-known function of macrophages is the removal of dead cells as part of tissue homeostasis but also following tissue injury[36]. We therefore endeavoured to characterise cell death dynamics in our model of cardiac regeneration as well as the requirement of macrophages in the removal of cellular debris.

Using the line *Tg(myl7:mKateCAAX;myl7:h2b-GFP)* that labels cardiomyocyte sarcolemma and chromatin respectively, we observed that following injury, a circlet of cardiomyocytes with pyknotic nuclei forms around the lesion site (Figure 3a). These pyknotic nuclei were TUNEL+ at 6 hpi, confirming apoptosis and mirroring the apoptotic border zone observed in mammalian infarcts[14,37] (Figure 3b). Interestingly, endogenous fluorescence is lost from the lesion as early as 0.5 hpi (Figure 3c). We hypothesised that the epicentre of the laser lesion may contain cells that immediately die upon injury by necrosis. To test this, the membrane-impermeable, fluorescent DNA intercalator propidium iodide (PI) was injected intravenously immediately following injury (<0.5 hpi) to label necrotic cells. We found that there were indeed PI+ cells in

the GFP- region and PI+ debris scattered across the proximal myocardium from 1 hpi (Figure 3d).

To discover how quickly this necrotic debris was cleared we used heartbeat-synchronised light sheet microscopy[38] to image the injured heart of PI-injected *Tg(mpeg1:GFP;myl7:h2b-GFP;myl7:mKateCAAX)* larva in timelapse. Necrotic cells are cleared rapidly within the first 0-2 hpi (Figure 3e, Video 3). We also observed condensed necrotic cells squeezing out from the myocardium into the pericardial cavity, independently of macrophage contact (Video 3). In a similar time-lapse experiment we imaged injured *Tg(myl7:mKateCAAX;myl7:h2b-GFP)* larva to see how quickly cells start to condense their nuclei as part of programmed cell death. We found that this too occurs extremely rapidly and is noticeable within just 1.5 hpi (Figure 3f, Video 4).

To test if macrophages aid in removal of damaged myocardium we performed time-lapse imaging at a later timepoint (4hpi) in injured *Tg(myl7:GFP;mpeg1:mCherry)* larvae. By 3D surface rendering the GFP+ cardiomyocytes and mCherry+ macrophages we observed small GFP+ pieces of debris near the GFP- lesion being removed and internalised by macrophages (Figure 3g, Video 5).

To determine if macrophages are required for the removal of apoptotic cells, we performed TUNEL staining on *irf8*-/- and *irf8*+/+ *Tg(myl7:h2b-GFP)* larvae at the standard 2, 6, 24, 48 hpi timepoints (Figure 3h &3i). In injured *irf8*+/+ hearts, the number of apoptotic cardiomyocytes significantly increased at 2 hpi and 6 hpi compared to uninjured controls (4.1±0.9 vs 0.0±0.0 and 5.3±1.0 vs 0.1±0.1 respectively). By 24 hpi, apoptotic cardiomyocytes are no longer significantly increased in injured *irf8*+/+ hearts (0.01±0.01 uninjured vs 0.2±0.1 injured). However, although injured macrophage-null *irf8*-/- hearts begin with a similar pattern of cell death at 2hpi and 6hpi (5.5±0.8 & 5.9±0.9 apoptotic cardiomyocytes respectively), apoptotic cardiomyocyte cells are still present at 24 hpi, returning to uninjured levels by 48 hpi.

In the macrophage ablation model, we saw a similar pattern of results where the numbers of apoptotic cells are negligible in uninjured hearts of all treatment groups

but peak at 6 hpi in injured groups (NTR+met-, NTR-met+ & NTR+met+ =6.4±0.5, 6.4±0.5 & 6.0±0.5) (Figure 3J). By 24 hpi the non-ablated control groups had no longer possessed significantly increased numbers of TUNEL+ myocardial cells (NTR+met- = 0.4±0.3 & NTR-met+ = 0.08±0.08) (Figure 3h & 3j). However, the injured macrophage-ablated group showed a retention of apoptotic cells at 24 hpi (NTR+met+ = 1.5±0.3) that resolved by 48 hpi. These results confirm the finding in the *irf8-/-* model that macrophages are required for the timely removal of apoptotic myocardial cells.

Macrophages are not required for structural or functional recovery of the heart

In adult zebrafish models of myocardial infarction there is full restoration of contractility and structure within 30-60 days[37]. It was therefore important to determine if there was full structural and functional recovery in the larval model of cardiac injury and if this was macrophage-dependent.

We lasered *Tg(myl7:GFP)* larvae in the macrophage ablation model. Using heartbeat-synchronised LSFM it was possible to acquire detailed 3D scans of cardiac structure of individual larvae across multiple timepoints (Figure 4a). In all treatment groups, the lesion remained the same size (~750μm^2) between 2 hpi and 6 hpi, with no difference between groups. By 24 hpi this lesion had almost completely regressed (95% to 37.1μm^2±24.4) in macrophage replete NTR+met- larvae (Figure 4b). However, in both the macrophage ablated NTR+met+ and the other macrophage replete NTR-met+ larvae, lesion closure was slightly delayed at 24 hpi (73% and 75% to 234.7±59.7 μm^2 and 221.4±84.6 μm^2 respectively). By 48 hpi the lesions of larvae from each group had entirely regressed and luminal surface renders of injured ventricles showed normal trabecular structure (Figure 4a). These results suggest macrophages are not required for lesion closure, but that metronidazole-treatment slightly delays this process.

We next sought to understand if this was also true of cardiac function. Again using *Tg(myl7:GFP)* larvae, we acquired lateral-view videos of beating hearts by epifluorescence, and calculated ventricular ejection fraction (Figure 4c &

Supplementary Figure 4a & 4b). Immediately following injury at 2 hpi ejection fraction is severely depressed in all groups from ~74% in uninjured ventricles to ~54% in injured. Ejection fraction recovers quickly by 6 hpi, with none of the treatment groups being significantly different to their respective uninjured controls but there still being a strong trend for injured larvae to have decreased ejection fraction (~78% injured vs 87% uninjured). At 24 hpi and 48 hpi this trend is also gone for all treatment groups and injured hearts are functionally indistinguishable from uninjured hearts. This data suggests that injured larval hearts recover their function rapidly and that this recovery is not macrophage dependent.

We next performed identical experiments examining the recovery of cardiac structure and function with *Tg(myl7:GFP)* larvae on an *irf8* mutant background. Both *irf8*+/+ and *irf8*-/- genotype larvae showed substantial lesion regression (~80%) between 6 hpi and 24 hpi (898.6 $\mu m^2 \pm 189.7$ to 211.6 $\mu m^2 \pm 115.8$ vs 1002.9 $\mu m^2 \pm 158.4$ to 113.89 $\mu m^2 \pm 59.5$ respectively) (Figure 4d & 4e). No difference in lesion size was seen at any timepoint and both genotypes had completely closed their lesions by 48 hpi. Normal trabecular structure was seen in both groups at 48 hpi following full structural recovery (Figure 4d). The recovery of ejection fraction in this model followed the same trend as that of the metronidazole-nitroreductase model, with the ejection fraction of injured larvae indistinguishable from uninjured larvae by 24 hpi in both genotypes (Figure 4e). Our near identical findings in the *irf8* macrophage null model confirm that larval hearts rapidly recover following laser injury and this is macrophage independent.

Finally, we wished to understand the mechanism of lesion closure, particularly how it was able to occur so rapidly following laser injury. We performed heart synchronised time-lapse imaging of lesions immediately following injury in *Tg(myl7:GFP)* larvae. Surface rendering of 3D scans of heart facilitated interpretation of morphological changes in myocardial volume (Figure 4g, Video 6). We observed GFP+ myocardial budding on opposite sides of the lesion border zone and subsequent invasion into the lesion, adhering to form a bridge. In order to ascertain if these buds and bridges represented individual pioneer cardiomyocytes, we repeated these live imaging experiments in *Tg(myl7:h2b-GFP;myl7:mKateCAAX)* larvae, facilitating the tracking of individual cardiomyocytes by virtue of their labelled nuclei and plasma membranes

(Figure 4h, Video 7). The initially disorganised surviving cardiomyocytes bordering the lesion began to extend protrusions into the lesion until they adhere with other single cardiomyocytes bridging from the opposing side of the lesion.

Macrophage ablation abolishes injury-associated increase in cardiomyocyte proliferation

To test if laser injury increases cardiomyocyte proliferation, we performed EdU staining in *Tg(myl7:h2b-GFP)* larvae in two experiments. The first where uninjured and injured larvae were exposed to EdU during 0-24 hpi and the second where the exposure occurs 24-48 hpi (Figure 5a). Analysis of the proportion of h2b-GFP+ with EdU incorporation immediately following the EdU pulse indicated the presence of cycling cardiomyocytes over both days (Figure 5b & 5c). EdU incorporation into cardiomyocyte nuclei was organ-wide, most often seen in pairs of cardiomyocytes but with no obvious distal or proximal localisation relative to the lesion (Figure 5b). Comparison between uninjured and injured hearts revealed no significant difference in the proportion of EdU+ cardiomyocyte nuclei 0-24 hpi (21.3±3.3 vs 18.9±3.4 respectively) (Figure 5c). However, over 24-48 hpi there was 35% increase in the proportion of EdU+ cardiomyocytes in injured hearts relative to uninjured (43.5±1.8% vs 32.2±2.0% respectively). Timelapse *in vivo* imaging of dividing cardiomyocytes showed nuclear division followed by cytokinesis, exclusively giving rise to mononuclear cells with no obvious hypertrophy (Video 8, Supplementary Figure 5a).

In order to understand if macrophages are required for the injury-dependent increase in cardiomyocyte proliferation we EdU pulsed only over the proliferative 24-48 hpi window in the macrophage-less models (Figure 5d). In the metronidazole-nitroreductase ablation model we found that the percentage of EdU+ cardiomyocytes increased in injured hearts in both the NTR+met- and NTR-met+ control groups but not in the macrophage-ablated NTR+met+ (Figure 5e & 5f). This result indicates that macrophages are a requirement for injury-dependent increase in cardiomyocyte proliferation. However, in contrast to the metronidazole-nitroreductase model, analysis of cardiomyocyte proliferation in *irf8-/-* mutants revealed that they too significantly increased the percentage of EdU+ cardiomyocytes following injury, comparably to

irf8+/+ larvae (Figure 5g & 5h). To resolve this disparity, we examined more closely the differences between these models. We found, like others, that *irf8-/-* mutants possess a greater global number of neutrophils than *irf8+/+* and mount a larger neutrophil response to injury (Supplementary Figure 5b & 5c). Since we do not observe an increased neutrophil response in NTR+met+ larvae, we hypothesised that neutrophils might be compensating for macrophages in *irf8-/-* larvae (Supplementary Figure 5d). To test this hypothesis, we inhibited neutrophil recruitment in *irf8-/-* larvae using a well-established antagonist 'SB225002' which blocks CXCR1/2 activation, a key chemokine receptor for neutrophil migration. CXCR1/2 inhibition successfully lowered the number of recruited neutrophils (2.0±3.4 vs 0.43±0.18) and abolished injury associated increase in cardiomyocytes in *irf8-/-* (Supplementary Figure 5e-g). Taken together this suggests that macrophages are important in inducing cardiomyocyte proliferation but are not an absolute requirement and can be substituted for by excess neutrophils.

Cardiac injury induces epicardial activation and VEGFaa upregulation

Macrophages are known to secrete a variety of growth factors and cytokines following cardiac injury but it is controversial whether these factors are directly required for cardiomyocyte proliferation *in vivo*[39,40]. We thought it plausible that macrophages may be releasing a key mitogen following laser injury. VEGFaa has recently been demonstrated to drive cell cycle entry in adult zebrafish following cryoinjury and is highly expressed in macrophages in larval trunk injury[21,41]. We hypothesised that macrophages may be promoting cardiomyocyte proliferation via the release of VEGFaa mitogen. Therefore we performed laser injury in *Tg(vegfaa:GFP;mpeg1:mCherry)* larvae to examine potential colocalised expression. However, no vegfaa expression was observed in macrophages at any timepoint, in uninjured or injured hearts (Supplementary Figure 6a & 6b).

In contrast, substantial vegfaa expression was observed in mesothelial cells overlying the myocardium (Figure 6a). Colocalisation with established epicardial marker tcf21 in *Tg(tcf21:DsRed;vegfaa:GFP)* larvae confirmed these cells to be early epicardium (Figure 5b). We tested if epicardial vegfaa:GFP expression increased still further

following larval cardiac injury by fluorescence intensity analysis of 3D *in vivo* imaging. vegfaa:GFP intensity increased significantly at 48 hpi with a strong trend to increase at 24 hpi (Figure 6d & 6e). Quantification of the total number of ventricular epicardial cells revealed that both the number of cells and their individual vegfaa:GFP expression increased following cardiac injury (Supplementary Figure 6c & 6d)

Macrophages localise to the epicardial niche and induce epicardial expansion

Since macrophages did not appear to express this known mitogen themselves, we wondered if their presence might be required to induce VEGFaa expression in epicardium. Supporting this hypothesis, detailed 3D analysis of macrophage localisation following injury showed recruited macrophages to synapse with epicardial cells by invading the myocardial-epicardial niche (Figure 6e). Given macrophage ablation abolishes injury-dependent cardiomyocyte proliferation (Figure 5f), we used metronidazole-nitroreductase model to ablate macrophages and assess whether epicardial activation still occurs following injury. We found that following injury, increased vegfaa:GFP expression was observed both NTR-met+ and NTR+met- groups but this failed to occur in NTR+met+ hearts, with vegfaa:GFP expression not significantly higher than in uninjured (Figure 6f & 6g). Interestingly, macrophage ablation did not affect vegfaa:GFP expression per cell but did block the expansion of epicardial cell number following injury (Figure 6h & Supplementary Figure 6e). Our data therefore suggests that recruitment of macrophages to epicardium is required for subsequent epicardial activation and expansion, as well to increase in net cardiac vegfaa expression.

VEGFaa is both required for, and sufficient for, cardiomyocyte proliferation in larval zebrafish

Although VEGFaa has been shown to be a potent inducer of cardiomyocyte hyperplasia in adult zebrafish and hypertrophy in adult mice, it is not known whether this is also true in larval zebrafish[41–43]. We first tested if VEGFaa alone is sufficient to stimulate cardiomyocyte proliferation in the absence of cardiac injury. Recombinant zebrafish VEGFaa protein (zfVEGFaa) or PBS control solution was microinjected into circulation via the sinus venosus of 72 hpf *Tg(myl7:h2b-GFP)* larvae and total

cardiomyocyte number assessed at 24 and 48 hpt (Figure 7a). A single injection of zfVEGFaa at 3 dpf increased total cardiomyocyte number by 13.3% relative to PBS-injected controls at 24 hpi (Figure 7b & 7c). Interestingly, by 48 hpt this is no longer statistically significantly different. This data confirms that VEGFaa is sufficient to stimulate hyperplasia in larval zebrafish hearts.

To test if VEGF signalling is required for the injury-associated cardiomyocyte proliferation, we used a pan-VEGFR receptor antagonist AV951 (Tivozanib) to block VEGF signalling. AV951 is a highly potent small molecule inhibitor and is widely used in larval zebrafish angiogenic assays as it can be easily delivered to tissues via bathing, commonly at concentrations of 500nM[44,45]. Our own validation and dose optimisation of VEGFR inhibition via a larval-laser trunk injury neovascularisation model[21] found AV951 could completely abolish neovascularisation in skeletal muscle at doses as low as 10nM (Supplementary Figure 7a-c). Consequently, we bathed larvae in 10nM AV951 dose over the course of our cardiac injury model, pulsing with EdU at 24-48 hpi and quantifying EdU+ cardiomyocytes at 48 hpi (Figure 7d). Interestingly, AV951 decreased the proportion of EdU+ cardiomyocytes in both the uninjured and injured groups (uninjured 38.4±3.4 vs 28.0±3.0 and injured 42.9±3.8 vs 31.6±2.2) (Figure 7e & 7f). This suggests that VEGF signalling in the heart is required for cardiomyocyte proliferation both as part of normal development and following cardiac injury. This agrees with our previous identification of constitutive epicardial VEGFaa expression in uninjured hearts.

Notch and Nrg-ErbB signalling are required for cardiomyocyte proliferation

Following the finding that VEGFR signalling is required for cardiomyocyte proliferation in both uninjured and injured hearts, we next sought to examine potential downstream effectors. Strong candidates were notch and neuregulin-ErbB signalling pathways. Notch signalling has been shown to be required for adult heart regeneration and cardiomyocyte proliferation in adult zebrafish[46–48] as well as in zebrafish heart development[49]. Neuregulin is a potent cardiac mitogen and has similarly been shown to be essential for adult regeneration as well as larval heart development[50–54].

Therefore, we first examined if either of these signalling pathways were required for cardiomyocyte proliferation in the larval heart following injury.

The gamma secretase inhibitor DAPT ((N-[N-(3,5-difluorophenacetyl)-l-alanyl]-S-phenylglycine t-butyl ester) has been successfully used as a pan-notch inhibitor for over two decades and has been demonstrated in both zebrafish and drosophila to phenocopy various notch mutants[55–57]. We performed the laser injury on *Tg(myl7:nlsDsRed)* larvae, bathing them in either 100µm DAPT or a vehicle control solution following injury and quantified total cardiomyocyte number at 48 hpi (Figure 7g). In agreement with previous studies, notch inhibition decreased cardiomyocyte number in uninjured hearts by ~8% (253.3±5.2 vs 233.4±4.5) (Figure 7h & 7i). Additionally, notch inhibition was similarly able to decrease cardiomyocyte number in injured hearts (266±5.6 vs 229±3.6). These results confirm that notch signalling is important for the expansion of cardiomyocyte number in both development and following cardiac injury.

We repeated this experiment, this time bathing larvae in an ErbB2 antagonist AG1478 (Figure 7e). Small molecule inhibitor AG1478 selectively inhibits ErbB2, required co-receptor for ErbB4 dimerization and subsequent neuregulin signal transduction. AG1478 is widely used in zebrafish cardiac biology to inhibit neuregulin-ErbB signalling[52,58–61], having been shown to faithfully phenocopy *erbb2* mutants[62]. Interestingly, the results exactly replicated those of the notch inhibition experiment, with decreased cardiomyocyte number in both uninjured (257.2±5.8 vs 235.2±4.2) and injured hearts (265.7±5.5 vs 229±5.9) (Figure 7j &7k). These results suggest that, like notch signalling, neuregulin-ErbB signalling is required for the expansion of cardiomyocyte number in both uninjured and injured settings.

Cardiac injury and VEGFaa induce endocardial notch signalling

Having demonstrated individual requirements for VEGF, notch and neuregulin-ERBB signalling, we were keen to test if they act in one pathway.

To reveal the epistatic relationship of these signalling components, we designed an experiment utilising the notch signalling reporter line *Tg(Tp1:venus-PEST)* as a readout of notch expression. The peptide sequence 'PEST' targets the fluorophore venus for rapid degradation and so increases temporal resolution of gene expression patterns. Recombinant zfVEGFaa or PBS control solution was injected into 3 dpf larvae and hearts analysed by heart-synchronised light-sheet microscopy for changes in notch signalling at 6, 24 and 48 hpi (Figure 8a). Furthermore, an additional group of larvae were injected with zfVEGFaa but also bathed in ErbB2 antagonist AG1478. We hypothesised a VEGFaa->notch->Nrg-ERBB pathway hierarchy (Figure 8b) and therefore reasoned that zfVEGFaa injection should upregulate notch signalling but that inhibition of Nrg-ErbB signalling should be unable to suppress zfVEGFaa-induced notch upregulation.

In agreement with previous studies[63,64] we found that in PBS-injected larvae, notch signalling was primarily in the endocardium, colocalising with endothelial reporter kdrl:mCherry, and in the occasional cardiomyocyte (Figure 8b). Notch signalling in larval cardiomyocytes has been recently shown to be the result of lateral inhibition during trabeculation whereas endocardial notch is known to drive cardiomyocyte proliferation[63]. Interestingly, endocardial notch signal was relatively low and only detectable in a subset of larvae at any given timepoint (Figure 8c). We therefore assessed if the percentage of hearts with Tp1:venus-PEST+ (notch+) endocardium increased following zfVEGFaa injection. zfVEGFaa injection significantly increased the percentage of notch+ endocardium from 46.4% to 78.6% at 6 hpi. Though there was a trend for the percentage of notch+ hearts to be higher in zfVEGFaa-injected larvae at 24 hpi (35.7% vs 17.9%), it did not reach statistical significance, nor was any difference observed at 48 hpi.

Treatment of zfVEGFaa-injected larvae with AG1478 failed to block the increase in the percentage of notch+ hearts. Furthermore, zfVEGFaa+AG1478 treated larvae had a substantially higher percentage of notch+ hearts at 48 hpi than those treated with zfVEGFaa alone (25.0% vs 0%). Together, these results show that VEGFaa is upstream of endocardial notch signalling and is that notch is unaffected by neuregulin-ErbB inhibition, excluding it from being downstream of the latter. Furthermore, the increased notch-signalling observed in zfVEGFaa+AG1478 hearts is highly suggestive

of negative-feedback, supporting the hypothesis that neuregulin might be downstream of notch as seen cardiac development.

Next, we sought to confirm if these signals interacted in a similar manner following injury; in particular whether injury alone could induce the same patterns of signalling. The experiment was repeated, substituting zfVEGFaa injection with laser injury (Figure 8e). As with zfVEGFaa injection, laser injury also increased the percentage of hearts with notch+ endocardium but this occurred later, at 48 hpi (50.0% vs 11.1%) (Figure 8f & 8g). Furthermore, there was also a strong trend for increased percentage of notch+ hearts in injured hearts relative to uninjured hearts at 24 hpi. Similar to zfVEGFaa injection, AG1478 did not block notch signalling, rather it seemed to enhance it. Whilst the percentage of notch+ hearts in the injured group did not significantly increase by 24 hpi, injured+AG1478 treated larvae did significantly increase relative to uninjured larvae (52.9% vs 11.1%). Furthermore, there was a trend for a greater percentage of notch+ hearts in injured+AG1478 treated larvae at 48 hpi compared to injured larvae alone (61.1% vs 50.0%). Taken together, these results demonstrate that endocardial notch signalling is downstream of cardiac injury and VEGFaa but is not downstream of Nrg-ErbB signalling, suggesting the latter is likely operating downstream of notch.

Regenerating larval hearts resolve inflammation and enter a reparative stage by 48 hpi

To understand what transcriptional changes are still occurring by the final timepoint of our model, we performed bulk RNAseq on pooled uninjured and injured larval hearts at 48 hpi (Figure 9a). We found a total of 1,464 differentially expressed (log_2 fold change >1) genes, 418 were upregulated in injured and 1,046 downregulated in injured hearts. We did not observe differential expression of canonical markers of proliferation such as MCM2, mKi67 and PCNA suggesting that the proliferation we observe from 24 hpi is concluded by 48 hpi (Figure 9b). In agreement with this, gene ontology analysis indicated categories such as growth factors and cell proliferation not to be enriched at 48 hpi (Supplementary Figure 9e). Although not differentially expressed at 48 hpi, many of the ligands and cognate receptors for VEGF, Nrg-ErbB

and notch were highly expressed in both uninjured and injured hearts indicating that these pathways are active in the larval heart (Supplementary table 1).

Most inflammatory and M1 markers were either not differentially expressed or downregulated in injured hearts, such as Il1b (Figure 9b & Supplementary file 1). In contrast, we found injury-associated upregulation of 39 collagen isoforms, and several profibrotic genes such as tgfb1a, osteopontin and markers of epithelial to mesenchymal transition (EMT) such as vimentin and twist2-3. Similarly, hierarchical clustering of differentially expressed genes revealed 9 distinct clusters with Cluster 1 being upregulated in injured hearts and enriched in collagens, matrix metalloproteins (MMPs) and fibroblast growth factors (FGFs) (Figure 9c, Supplementary file 2). Additionally, Cluster 2 contained several EMT genes, Cluster 8 genes relating to cell recruitment and lymphagiogeneis whilst Cluster 7 contained several embryonic-associated myosins and myosin binding proteins such as myl10, myl13 and cald1b. Clusters 3-6 & 9 were downregulated in injury, Cluster 2 was enriched for immune genes and Clusters 4 and 6 for growth factors, with Clusters 3 and 5 less easily described.

Taken together, our RNAseq results suggest that the inflammatory and proliferative stages are largely concluded by 48 hpi and that a pro-resolving, reparative and remodelling phase dominates from this timepoint.

Discussion

In this study we present a detailed characterisation of the larval zebrafish model of heart regeneration, demonstrating the heterogeneity and plasticity of macrophages in cardiac injury and testing the requirement of macrophages for the removal of apoptotic cells, cardiomyocyte proliferation, epicardial activation and recovery of cardiac structure and function. Furthermore, we demonstrate the utility of the larval cardiac injury model by taking advantage of it's *in vivo* cardiac imaging opportunities and amenability to pharmacological intervention to suggest a novel role for macrophages in driving cardiomyocyte proliferation via epicardial activation.

Recent zebrafish studies examining macrophages in other wound contexts, such as spinal cord and tail transection, have demonstrated tnf-α to mark M1-like macrophages, that then transition to M2-like macrophages[18,30,65]. Similarly, studies in the adult zebrafish heart have shown the presence of a subsets stratified on the basis of tnf-α, wt1b, csf1ra and mpeg1 transgenic reporter expression[29,34]. We confirmed the presence of mpeg1+csf1ra+ and mpeg1+csf1ra- subsets in larval heart injury, finding as in adults that these cells have identical recruitment dynamics and no obvious differences in morphology or behaviour[34]. Recent Cre-Lox lineage tracing has shown that mpeg1+csf1ra- cells have a non-haematopoietic origin, are csfr1a-independent developmentally and unlike mpeg1+csf1ra+ cells, are not phagocytic[66,67]. Due to their non-haematopoietic origin some have termed mpeg1+csf1ra- cells as 'metaphocytes' rather than macrophages however macrophage ontogeny is diverse and environment is known to play a leading role in establishing macrophage identity[27,68]. Therefore, further functional analysis and transcriptomic clustering relative to other immune cells is required to classify mpeg1+csf1ra- macrophages as a non-macrophage cell type.

Our observation of a transient tnfα+ subpopulation is in agreement with findings in the adult cryoinjury and larval tail-transection models[30,34]. Our success in increasing the percentage of tnf-α+ macrophages by canonical M1-polarising cytokine IFN-γ-rel suggests that early tnf-α+ macrophages are proinflammatory. Furthermore, we used heart synchronised live imaging to show that macrophages can convert from mpeg1+tnf-α- to mpeg1+tnf-α+. This is the first time that macrophages have been imaged converting phenotype in the heart and provides direct evidence of plasticity as opposed to recruitment of heterogenous subsets. Our RNAseq data confirmed the inflammatory response to be transient as by 48 hpi hearts downregulate inflammatory cytokines and growth factors but upregulate collagens and reparative cytokines. Our finding that the a fibrotic program is activated in injured hearts despite full structural and functional recovery is in agreement with a recent study showing the scar-deficient runx1-/- zebrafish to undergo successful cardiac regeneration[69]. It might be that the fibrotic program is concomitantly activated upon the resolution of inflammation.

We used two separate methods to examine the effect of removing macrophages from the larval heart injury model. By using two methods we hoped to control for potential

595 artefacts of the techniques. Cell death data acquired by either technique demonstrated
596 that macrophages are required for the removal of apoptotic cells following injury.
597 Furthermore, we found that the structure of laser lesions was analogous to that of
598 human infarcts and adult zebrafish cryoinjury with a necrotic core surrounded by
599 apoptotic cardiomyocytes and border zone[6,37]. Interestingly, these cells do eventually
600 seem to be cleared even in the absence of macrophages. Our live imaging showed
601 that dead cardiomyocytes can be expelled from the myocardium independently of
602 macrophages. It is possible that this is a mechanical consequence of cardiac
603 contraction however a similar phenomenon is known to occur in neuroepithelium
604 where neurons appear to extrude apoptotic cells out of tissue[70,71]. Nevertheless, we
605 were also able to image, for the first time, macrophages actively removing and
606 internalising myocardial material following cardiac injury.
607
608 Surprisingly, we found that the absence of macrophages in neither macrophage-less
609 model had any effect on the structural or functional recovery of the injured larval heart.
610 This is in contrast to previous studies in mice where macrophage depletion leads to a
611 reduced ejection and infarct expansion [23,72,73]. Likewise, liposomal clodronate
612 macrophage ablation and CCR2-antagonist inhibition of macrophage recruitment in
613 regenerative neonatal mice, zebrafish and axolotl hearts causes blocked or delayed
614 resolution of the infarct area[15,16,74]. The contrasting results in the larval heart might
615 simply be a consequence of its small size and low transmural pressure. Furthermore,
616 the diameter of the infarct is only 1-2 cells, allowing surviving bordering
617 cardiomyocytes to restore the myocardial syncytium without prior proliferation. Indeed,
618 we observed individual cardiomyocytes extending protrusions into the lesion. Previous
619 histological analysis of the border zone in injured adult zebrafish and neonatal mouse
620 hearts has shown cardiomyocytes exhibiting a similar mesenchymal phenotype
621 following partial dedifferentiation and disassembly of sarcomeres.[75–77]. To our
622 knowledge, this is the first time this behaviour has verified directly by time-lapse
623 imaging live in a beating heart.
624
625 Studies in adult zebrafish and neonatal mice have shown ablation of macrophages to
626 decrease cardiomyocyte proliferation, the exception being axolotls where it has no
627 effect[15,17,40,78,79]. Additionally, cardiomyocyte proliferation and macrophage
628 recruitment dynamics correlate and enhancement of macrophage recruitment in the

non-regenerative teleost medaka, facilitates cardiomyocyte proliferation and regeneration[17,78]. However, early revascularisation is critical for cardiomyocyte proliferation and is macrophage-dependent calling into question whether macrophages directly induce cardiomyocyte proliferaiton[17,80]. Our larval model provided a unique opportunity to uncouple the angiogenic actions of macrophages from cardiomyocyte proliferation since larval hearts do not have supporting vasculature at this stage[32]. The increased proliferation we observed following injury demonstrates that larval hearts are truly regenerating and not recovering via normal developmental growth. Furthermore, macrophage ablation completely abolished the injury-dependent cardiomyocyte proliferation seen in macrophage replete hearts, suggesting this effect is might not be entirely mediated by revascularisation in other models. Interestingly, *irf8-/-* larvae still exhibit a robust proliferative response to injury. In line with previous studies, we found that *irf8-/-* and not macrophage-ablated larvae showed increased recruitment of neutrophils[18,33]. Pharmacological inhibition of neutrophil recruitment abolished expansion of cardiomyocyte number suggesting that large neutrophil response can compensate for the absence of macrophages.

Zebrafish macrophages have been shown to upregulate VEGFaa following injury of trunk intersegmental vessels and VEGFaa has also been shown to be a powerful mitogen for cardiomyocytes in adult cryoinjury[21,41]. However, macrophages were not VEGFaa+ in the vegfaa:GFP reporter line. We instead found that VEGFaa is constitutively expressed in larval epicardium[41,81]. Pharmacological inhibition of VEGFR signalling decreased cardiomyocyte proliferation in uninjured larvae and in injured larvae who show an increase in expression of VEGFaa. This provides a mechanism for epicardial driven cardiomyocyte proliferation. Confirming this, a single intravenous injection of recombinant zfVEGFaa substantially increased the number of cardiomyocytes in hearts at 24 hpt. Interestingly, control hearts appear to match this increase by 48 hpt. It is possible that endogenous VEGFaa is therefore acting as a trigger to cardiomyocytes competent to divide and that injection of zfVEGFaa triggered the majority of these competent cardiomyocytes to divide ahead of developmental schedule.

Although macrophages do not express VEGFaa themselves following cardiac injury, their presence appears to be required for injury-dependent upregulation of mitogen

VEGFaa via the expansion of the epicardium. Furthermore, we showed that macrophages specifically home to the myocardial-epicardial niche. This is reminiscent of previous findings in developing and injured mouse hearts where yolk-derived and Gata6+ pericardial cavity macrophages are recruited to the epicardium, respectively[82,83]. Future studies should seek to identify precisely how macrophages activate epicardium. Given we found that elevated neutrophil recruitment can induce cardiomyocyte proliferation in the absence of macrophages, epicardial activation might be induced by a shared inflammatory factor.

We showed both notch and Nrg-Erbb signalling to be required for expansion of cardiomyocyte numbers in both uninjured and injured heart. This is in agreement with previous findings in adult zebrafish and murine models[46–48,51,58]. Interestingly, our data demonstrated that both VEGFaa and injury increase endocardial notch signalling. Endocardial notch1b is known to regulate maturation of the larval ventricle via downstream Nrg1[49]. Therefore, it was plausible that a VEGF>Notch>Nrg-ErbB pathway might be inducing cardiomyocyte proliferation in the larval cardiac injury model. A recent paper published during the course of this study demonstrated exogenous VEGF to be capable of inducing cardiomyocyte hypertrophy in the mouse heart via a VEGF>notch>nrg1 pathway[43]. Whilst unconfirmed in models of MI, it raises the possibility that this could represent an injury-dependent recapitulation of developmental growth programming, conserved between regenerative and non-regenerative animals. Given the angiogenic effects of VEGFaa, our proposed pathway would present an elegant coupling revascularisation to myocardial growth, under the control of macrophage inflammation. Future studies are required to determine if this pathway is similarly active in adult zebrafish and mammalian hearts and understand precisely how macrophages are inducing upstream epicardial activation.

Materials and Methods

Zebrafish husbandry and lines used

Zebrafish husbandry and maintenance was conducted as per standard operating procedures, in accordance with the Animals (Scientific Procedures) Act, 1986 and

approved by The University of Edinburgh Animal Welfare and Ethical Review Board in a United Kingdom Home Office-approved establishment. All our experiments were performed on staged zebrafish aged between 3 dpf and 5 dpf[84]. The following transgenic and mutant lines were used: *Tg(myl7:eGFP)*^{twu26} [85], *Tg(mpx:mCherry)*^{uwm7} [86], *Tg(mpeg1:mCherry)*^{gl23} [87], *Tg(mpeg1:eGFP)*^{gl22} [87], (*Tg(mpx:GFP)* ^{i114} [88], *Tg(myl7:h2b-GFP)*^{zf52} [89], *Tg(myl7:mKateCAAX)*^{SD11} [90], *Tg(fms:Gal4.VP16)*^{i186}, referred to as csfr1a:gal4[91], *Tg(UAS-E1b:NfsB-mCherry)*^{c264} abbreviated to UAS:NfsB-mCherry[92], *Tg(vegfaa:eGFP)*^{PD260} [41], *Tg(myl7:nlsDsRed)*^{f2} [93] *Tg(TNFa:eGFP)*^{sa43296} [30], *Tg(Tp1:venus-PEST)*^{S940} [94], *Tg(kdrl:hsa.HRAS-mCherry)*^{S896} [95], *Tg(kdrl:GFP)*^{la116} [96], *Tg(tcf21:DsRed)*^{PD37} [97], *Tg(myl7:gal4:myl7:GFP)*^{cbg2Tg} [98], *Tg(UAS:mRFP)*[99] and irf8$^{st95/st95}$ [33] referred to as *irf8-/-*. Adults were day-crossed as appropriate to yield desired combinations of transgenes in embryos. Embryos were treated with 0.003% phenylthiourea (Fisher Scientific) at 7 hpf to prevent pigment formation and therefore enhance image clarity[100]. Embryos and larvae were incubated at 28.5°C in conditioned media/water (6.4 mM KCl, 0.22 mM NaCl, 0.33 mM $CaCl_2{\cdot}2H_2O$, 0.33 mM $MgSO4{\cdot}7H_2O$) + 0.1% methylene blue (w/v) and imaged at room temperature (23°C) using epifluorescence or light sheet fluorescence microscopy (details below). When necessary, larvae were anesthetized using 40 µg/ml tricaine methanesulfonate (Sigma Aldrich) in conditioned media.

Cardiac laser injury

A Zeiss Photo Activated Laser Microdissection (PALM) laser system (Zeiss) was used to precisely cause a localised injury at the ventricular apex of anesthetized 72 hpf larvae[32]. Larvae were mounted on a glass slide in 20 µl anesthetized conditioned media and lasered via a 20X objective. Injuries were deemed successful and complete once ventricular contractility decreased, the apex had shrunk, and the myocardial wall had swollen without causing cardiac rupture and subsequent bleeding. A successful cardiac injury results in the portion of dysfunctional tissue losing fluorescent myocardial transgenic fluorescence signal. Uninjured larvae were treated in the same manner up to the point of laser injury, when they were individually transferred into single wells of a 24-well plate and maintained in the same environmental conditions as injured fish.

731 **Epifluorescence microscopy**

732

733 Larvae were mounted laterally in conditioned media on a glass slide and imaged using
734 a Leica M205 FA stereomicroscope with GFP and mCherry filters. For all serial
735 timepoint epifluorescence imaging experiments, number of immune cells on the heart
736 were quantified by manually observing and counting cells moving synchronously with
737 the beating heart. Heart images were acquired using 16X objective. The number of
738 immune cells at the tail were quantified by counting from the caudal end of the vascular
739 loop to the wound edge as performed by others[32,101]. Tail images were acquired using
740 8X objective. CHT and trunk vasculature images were acquired using a 6X objective.
741 Whole larva images were acquired using 2.5X objective.

742

743 **Heart-synchronised light-sheet microscopy**

744

745 Individual larvae were prepared for light sheet fluorescence microscopy (LSFM) by
746 embedding in 1% low melting-point agarose (ThermoFisher) in anesthetized
747 conditioned media inside FEP tubes (Adtech Polymer Engineering). Agar embedding
748 prevents gradual drift of the embryo in the FEP tube, without causing developmental
749 perturbations during long-term imaging. Larvae were used only once for a timelapse
750 imaging experiment, and any repeats shown come from distinct individuals. Larvae
751 were mounted head down such that the heart faces toward both illumination and
752 imaging objectives to improve image clarity. All LSFM experiments were performed at
753 room temperature (23°C). Exposures ranged from 5-15 ms and frequency of scans
754 were 3-5 minutes. Brightfield images acquired at 80 fps were used to inform the optical
755 gating and acquire z slices in a set phase of cardiac contraction, usually mid diastole.
756 The setup of our custom-built LSFM system has been previously reported in detail[38].

757

758 **Metronidazole-nitroreductase macrophage ablation model**

759

760 In order to selectively ablate macrophages prior to cardiac injury, embryos were
761 treated incubated as previously described until 48 hpf and then treated as follows.
762 Embryos were carefully dechorionated at 48 hpf and screened based on fluorescence
763 and split into groups appropriate to the experiment, for example larvae were always
764 split into csf1ra:gal4;UAS:NfsB-mCherry+ and csf1ra:gal4;UAS:NfsB-mCherry-.

Embryos were then transferred to either conditioned water or a 0.5mM metronidazole (Thermo Fisher Scientific) solution, both solutions also contained 0.003% phenylthiourea (Thermo Fisher Scientific) and 0.2% DMSO (Sigma Aldrich). Larvae were then incubated in these solutions in the dark at 28. 5°C for 24 hours prior to injury at 72 hpf. Larvae were then removed from the metronidazole solution and vehicle solution and placed in fresh conditioned water + 0.003% phenylthiourea for the remainder of the experiment. As shown in Figure 2 and Supplementary Figure 2, this is sufficient to ablate macrophages prior to injury and completely block subsequent macrophage recruitment to the injured heart.

Neutral red staining

Larvae were incubated at 72 hpf in 5ug/mL neutral red in conditioned water for 5 hours in the dark at 28.5°C. Larvae were then washed twice for 5 minutes in conditioned water, anaesthetised with 40 µg/ml tricaine methanesulfonate and imaged by brightfield microscopy on a Leica M205 FA stereomicroscope.

Genotyping of *irf8-/-* mutants

Adult (>30 dpf) zebrafish arising from heterozygous *irf8* mutant incrosses were anaesthetised in 40 µg/ml tricaine methanesulfonate and a lobe of caudal fin removed by scalpel. After clipping, fins were digested to extract DNA using 10mg/ml Prot K, incubated at 65oC for 1 hr. This incubation ends with 15 minutes at 95ºC to denature the Proteinase K. A section of irf8 flanking the mutation locus was then amplified from the extracted DNA by PCR using Forward -ACATAAGGCGTAGAGATTGGACG and Reverse -GAAACATAGTGCGGTCCTCATCC primers and REDTaq® ReadyMix™ PCR Reaction Mix. The PCR product was then digested for 30 mins at 37 ºC using AVA1 restriction enzyme (New England Bioscience) and the product run on a 2% agarose gel. WT = AvaI digest site is present = PCR product is cleaved to give two bands with sizes of approximately 200 and 100 bp. irf8 -/- = AvaI digest site is absent due to mutation = PCR product is not cut. A single band is observed with a size of 286 bp. irf8 +/- = Three bands as above.

Microinjection recombinant proteins and intravital stains

Microinjections were performed on larvae at 72 hpf using a Narishige IM-300 Microinjector and pulled thin wall glass capillaries (Harvard Apparatus), administered under anaesthesia by intravenous microinjection through the cardiac sinus venosus (SV) that drains the common cardinal vein (CCV). An injection volume of 1 nL was used for all intravenous injections to minimise disruption to blood volume.

For propidium iodide intravital staining, 1nL 100µg/ml propidium iodide in DPBS was injected immediately following injury at 0.5 hpi. Larvae were then immediately imaged by heart synchronised light-sheet microscopy at 1 hpi. Injection of recombinant zfIFN-γ-rel (IFN-1.1) (Kingfisher Bioscience) was administered as a single 1nL 132nM dose at 72 hpf. Lyophilised IFN-γ-rel was reconstituted in PBS + 0.1% BSA (carrier protein) and PBS + 0.1% BSA was used as the vehicle control solution. Injections of recombinant zfVEGFaa (Kingfisher Bioscience) were administered as single 1nL 0.25 ug/ul doses at 72 hpf (protein reconstituted as above).

Trunk laser injury and neovascularisation

A Zeiss Photo Activated Laser Microdissection (PALM) laser system (Zeiss, Oberkochen, Germany) was used to precisely cause a localised injury to the skeletal muscle segment directly dorsal to the posterior end of the cloaca in anesthetized 72 hpf larvae. Care was taken not to damage the intersegmental vessels. Muscle can seen to be successfully injured by disruption of its usually smooth striated appearance via monitoring in brightfield. Additionally, successfully injured larvae will be paralysed for approximately 24 hpi due to the proximity of the spinal cord. Uninjured larvae were treated in the same manner up to the point of laser injury, when they were individually transferred into single wells of a 24-well plate and maintained in the same environmental conditions as injured fish. Larvae were then incubated until 48 hpi 28.5°C in conditioned media/water + 0.1% methylene blue + (W/V) 0.003% phenylthiourea (Thermo Fisher Scientific) and imaged at room temperature (23°C) using epifluorescence. At 48 hpi, neovasculature can be visualised by *kdrl:GFP* fluorescence to have invaded the injured skeletal muscle in a portion of injured larvae. The total length of the neovascular network can be quantified post-acquisitionally by image analysis in FIJI (National Institutes of Health).

833

834 **Tail fin transection injury**

835

836 The tail/caudal fin of anesthetized 72 hpf larvae was transected using a sterile scalpel,
837 avoiding damage to the end of the notochord and vasculature and as previously
838 reported[102]. Uninjured (control) fish were treated in the same manner up to the point
839 of transection, when they were separated into a 24-well plate and maintained in the
840 same environmental conditions as injured fish.

841

842 **Histological staining**

843

844 To detect cell death at the injured ventricle, whole-mount larval TUNEL staining was
845 performed. Larvae were fixed in 4% PFA for 30 mins and transferred to 1:10 dilution
846 of PBS. Larvae were subsequently digested in 1 µg/ml Proteinase K for 1 h. Larvae
847 were re-fixed in 4% PFA for 20 mins and subsequently washed in PBT. TUNEL
848 staining was performed using ApopTag Red In situ kit (MilliporeSigma) to label
849 apoptotic cells, as described previously[32]. Stained hearts were imaged using LSFM.

850

851 EdU staining was performed by incubating larvae in 1mM EdU (5-ethynyl-2′-
852 deoxyuridine) (Abcam) in 1 % DMSO (Sigma Aldrich) in conditioned water + 0.003%
853 phenylthiourea (Thermo Fisher Scientific) for 24 hours beginning either at 0 hpi or 24
854 hpi depending on the experiment. Larvae were incubated at 28.5°C in the dark. Larvae
855 were then fixed for 2 hours at room temperature in 4% PFA, permeabilised in
856 permeabilisation solution (PBS-Triton-X 0.1% + 1% Tween + 1% DMSO) and
857 pericardium punctured using a glass microinjection needle (further improving
858 permeability). Larvae were then washed twice in PBS-3% BSA and incubated for 2
859 hours at room temperature in CLICK reaction mixture from Click-iT™ EdU Imaging Kit
860 with Alexa Fluor™ 594 (Invitrogen) made according to manufacturers' instructions.
861 Larvae were finally washed once in PBS-3%BSA and twice in PBS-0.1% tween and
862 imaged by LSFM.

863

864 **Heart lesion size quantification**

865

Larval hearts expressing the transgene *myl7:GFP* were imaged by heart-synchronised light-sheet imaging as described above. Exposure was kept consistent at 10ms as well as z slice spacing (1 μm) and heart contraction phase was locked to mid diastole for all larvae. Z stacks were surface rendered in IMARIS (Bitplane) based on absolute intensity and software-suggested segmentation and rendering parameters. Lesion area, visualised as a render-free hole in the myocardium, was then traced around manually and lesion area quantified in FIJI (National Institutes of Health).

Ventricular ejection fraction analysis

Larval hearts of *Tg(myl7:GFP)* larvae were imaged at 80 fps in brightfield using a Leica M205 FA epifluorescence stereomicroscope to capture when the ventricle was in diastole and systole. The ventricular area in diastole and systole was measured manually in FIJI and ventricular ejection fraction calculated using the formula 100 X [(Diastolic Area – Systolic Area)/Diastolic Area][31]. Ventricular ejection fraction by area was then converted to ejection fraction by volume using the formula 'Ejection fraction by area x 2.33 = Ejection fraction by volume' derived in Supplementary Figure 4. Over the small range of ejection fractions that occur in larval hearts, the relationship can be considered to approximate to a linear one.

Quantification of cell number by image analysis

To quantify the number of cardiomyocytes in *Tg(myl7:h2b-GFP)* and *Tg(myl7:nlsDsRed)* larval hearts z stacks of hearts acquired by LSFM were imported into FIJI and nuclei counted by the plugin Trackmate. Briefly, key segementation parameters 'Estimated blob diameter'=5.5, 'Threshold'=0.9 were taken as a starting point and optimised manually per experiment until all nuclei are counted successfully. The heart atrium is excluded manually by x coordinate filtering and ventricular cardiomyocytes are then automatically by the plug in.

In order to automatically quantify the percentage of EdU+ ventricular cardiomyocytes in *Tg(myl7:h2b-GFP)* larval hearts a custom FIJI macro was written to exclude non-cardiomyocyte EdU signal. This is necessary as cardiomyocytes have a much lower turnover rate than surrounding cells in the pericardium, endocardium and blood and

so represent a minority of EdU+ cells. Briefly, the Bersen segmentation method was used to mask areas of GFP fluorescence per z slice and these masks subsequently applied as a crop ROI to EdU signal in the 564 (red) channel of RGB images. Slices were then reassembled and merged into maximum intensity projections where the FIJI Trackmate plugin was used to count both the total number of GFP+ cardiomyocyte nuclei and EdU+ cardiomyocyte nuclei. This quantification then allowed the percentage of EdU+ cardiomycytes to be calculated in an unbiased way per larval heart.

Quantification of notch signalling by image analysis

In order to objectively identify whether the hearts from *Tg(Tp1:venus-PEST)* larvae possessed venus signal in the endocardium above that of background, and were therefore 'notch+', the following approach was used. Treatment groups were blinded to the analyser and z stacks opened in FIJI. The automatic brightness and contrast function was used to objectively enhance the signal in the heart and the clear interface between the granular autofluorescence of the chamber blood and the smooth autofluorescence of the myocardium searched for venus expression. The distinctive morphology and location of endothelium allowed for unambiguous identification of venus+ status.

For the quantification of the total myocardial *Tp:venus-PEST* fluorescence, z stacks were blinded and processed in FIJI. Stacks were converted to maximum intensity projections and a standardised size ROI was manually positioned over the notch^{high} atrioventricular valve allowing it to be cropped out of the image and preventing it from interfering with myocardial signal. This is because during development it exhibits exceptionally high *Tp1:venus-PEST* fluorescence, unlike the endocardium whose fluorescence is negligible relative to the myocardium. Ventricles were then manually traced, avoiding the bulbous arteriosus as it is similarly notch^{high} during development and fluorescence summed. Fluorescence was then normalised by subtracting background fluorescence of venus-negative larvae imaged similarly.

Pharmacological inhibition of larval signalling

To inhibit VEGF signalling larvae were bathed in pan-VEGFR antagonist AV951/Tivozanib (Stratech Scientific) 0-48 hpi. AV951 was dissolved in 0.1% DMSO in conditioned water + 0.003% phenylthiourea to make a 10nM solution, with just 0.1% DMSO in conditioned water + 0.003% phenylthiourea becoming the vehicle control. In order to pulse larvae with EdU, the orginal solution was replaced the same solution was except for the addition of 1mM EdU at 1% DMSO.

To inhibit notch signalling, larvae were bathed in gamma secretase inhibitor DAPT (Cambridge Bioscience) 0-48 hpi. DAPT was dissolved in 0.2% DMSO in conditioned water + 0.003% phenylthiourea to make a 100μM solution, with just 0.2% DMSO in conditioned water + 0.003% phenylthiourea becoming the vehicle control. Note, DAPT must be dissolved in DMSO prior to the addition of water to prevent precipitation.

In order to inhibit neuregulin-ERBB signalling, the ErBB2 antagonist AG1478 was used. Larvae were bathed in 1.75 μM AG1478 (Cambridge Bioscience) dissolved in 0.25% DMSO in conditioned water + 0.003% phenylthiourea over 0-48 hpi.

Extraction of larval hearts and RNA extraction

Following laser injury at 72 hpf *Tg(myl7:gal4::GFP;UAS:mRFP)* larvae were incubated at 28.5°C in conditioned media/water + 0.1% methylene blue (w/v) + 0.003% phenylthiourea. At 48 hpi uninjured and injured larvae were given an overdose of tricaine at 400 μg/ml, following which hearts were extracted. We adapted the protocol of Burns and MacRae[103] to increase the yield of heart retrieval from ~50% to ~70%. Briefly, ~30 larvae were placed in 2mL eppendorf tubes, the conditioned water drained and replaced with ice cold Leibovitz's L-15 Medium supplemented with 10% FCS. A 19-gauge needle coupled to a 5mL syringe was used to shear the larvae by aspiration and therefore dissociate hearts from the rest of the larva. The lysate was then inspected by epifluorescence microscopy and mRFP+ hearts and collected to be kept on ice. Hearts were then digested at for 10 minutes at 4°C in protease solution (5 mM CaCl2,10 mg/ml B. Licheniformis protease, 125 U/mL DNase I in 1x PBS) with occasional aspiration to aid digestion (Truong et al,). RNA was then extracted using a RNeasy Plus Micro Kit (Qiagen) following direct lysis with RLT lysis buffer according

to manufacturer's instructions. RNA concentration was measured by Qubit and integrity by Bioanalyser. RIN score for all samples ranged between 9.6-10.

RNAseq analysis

RNA was sequenced by Genewiz, Leipzig, Germany by Illumina NovaSeq, PE 2x150. Genewiz also used eseq2 package was used in R to evaluate sequencing quality, trim reads, map to the *Danio rerio* genome and generate gene counts/hits. Sequence reads were trimmed using Trimmomatic v.0.36. The trimmed reads were mapped to the Danio rerio GRCz10.89 reference genome available on ENSEMBL using the STAR aligner v.2.5.2b. Unique gene hit counts were calculated by using featureCounts from the Subread package v.1.5.2. Only unique reads that fell within exon regions were counted. The Wald test was used to generate p-values and log2 fold changes. A gene ontology analysis was performed on the statistically significant set of genes by implementing the software GeneSCF v.1.1-p2. The zfin GO list was used to cluster the set of genes based on their biological processes and determine their statistical significance. The volcano plot was generated by a custom R script and heatmap constructed using the pHeatmap package. For the heatmap z scaled log2(Reads) were clustered via Pearson correlation and clusters thresholded based on the resulting dendrogram. The heatmap was generated using the pHeatmap function in R.

Statistics

Graphs and statistics were curated in GraphPad Prism 9.1 software (GraphPad Software). Data were analyzed by student *t*-test, one-way ANOVA or two-way ANOVA followed by an appropriate multiple comparison *post hoc* test. All statistical tests, *p*-values and *n* numbers used are given in figure legends.

Acknowledgments

This work was funded by a British Heart Foundation (BHF) CoRE award (RE/13/3/30183), Medical Research Scotland studentship (PhD-1049-2016), NC3R studentship (NC/P002196/1), BHF New Horizons grant (NH/14/2/31074), and a Medical Research Council UK award (MR/K013386/1). Bioinformatics and RNAseq performed by Genewiz, Leipzig, Germany. We also acknowledge Amelia Edmondson-Stait, University of Edinburgh, for her advice and input on RNAseq analysis.

Author Contributions

FAB conceived of and designed the study. FAB, AK and GM carried out all experiments. Image analysis was performed by FB and AK. LSFM-related technical assistance was provided by JMT. FAB wrote the manuscript. KRS, EGS and MB provided expertise regarding all RNA work. KRS helped optimise larval heart extraction and RNA extraction. JMT, CST, JJM, GM, MB, AGR, and MAD edited the manuscript. MAD, AGR, and CST supervised the study. All authors contributed to the article and approved the submitted version.

References

1. Ohnmacht, J., Yang, Y., Maurer, G. W., Barreiro-Iglesias, A., Tsarouchas, T. M., Wehner, D., Sieger, D., Becker, C. G. & Becker, T. Spinal motor neurons are regenerated after mechanical lesion and genetic ablation in larval zebrafish. *Dev.* **143**, 1464–1474 (2016).
2. Becker, C. G., Lieberoth, B. C., Morellini, F., Feldner, J., Becker, T. & Schachner, M. L1.1 is involved in spinal cord regeneration in adult zebrafish. *J. Neurosci.* **24**, 7837–7842 (2004).
3. Bensimon-Brito, A., Ramkumar, S., Boezio, G. L. M., Guenther, S., Kuenne, C., Helker, C. S. M., Sánchez-Iranzo, H., Iloska, D., Piesker, J., Pullamsetti, S., Mercader, N., Beis, D. & Stainier, D. Y. R. TGF-β Signaling Promotes Tissue Formation during Cardiac Valve Regeneration in Adult Zebrafish. *Dev. Cell* **0**,

(2019).

4. Sander, V., Davidson, A. J., Sander, V. & Davidson, A. J. Kidney Injury and Regeneration in Zebrafish. *Semin. Nephrol.* **34**, 437–444 (2014).
5. Basu Mallik, S., Jayashree, B. S. & Shenoy, R. R. Epigenetic modulation of macrophage polarization- perspectives in diabetic wounds. *J. Diabetes Complications* **0**, (2018).
6. González-Rosa, J. M., Martín, V., Peralta, M., Torres, M. & Mercader, N. Extensive scar formation and regression during heart regeneration after cryoinjury in zebrafish. *Development* **138**, 1663–1674 (2011).
7. Leuschner, F., Rauch, P. J., Ueno, T., Gorbatov, R., Marinelli, B., Lee, W. W., Dutta, P., Wei, Y., Robbins, C., Iwamoto, Y., Sena, B., Chudnovskiy, A., Panizzi, P., Keliher, E., Higgins, J. M., Libby, P., Moskowitz, M. A., Pittet, M. J., Swirski, F. K., Weissleder, R. & Nahrendorf, M. Rapid monocyte kinetics in acute myocardial infarction are sustained by extramedullary monocytopoiesis. *J. Exp. Med.* **209**, 123–37 (2012).
8. Murry, C. E., Reinecke, H. & Pabon, L. M. Regeneration Gaps. Observations on Stem Cells and Cardiac Repair. *Journal of the American College of Cardiology* vol. 47 1777–1785 (2006).
9. Bergmann, O., Zdunek, S., Felker, A., Salehpour, M., Alkass, K., Bernard, S., Sjostrom, S. L., Szewczykowska, M., Jackowska, T., dos Remedios, C., Malm, T., Andrä, M., Jashari, R., Nyengaard, J. R., Possnert, G., Jovinge, S., Druid, H. & Frisén, J. Dynamics of Cell Generation and Turnover in the Human Heart. *Cell* **161**, 1566–1575 (2015).
10. Pfeffer, M. A. & Braunwald, E. Ventricular remodeling after myocardial infarction. Experimental observations and clinical implications. *Circulation* **81**, 1161–72 (1990).
11. Richardson, W. J., Clarke, S. A., Quinn, T. A. & Holmes, J. W. Physiological Implications of Myocardial Scar Structure. *Compr. Physiol.* **5**, 1877–909 (2015).
12. Jopling, C., Sleep, E., Raya, M., Martí, M., Raya, A. & Belmonte, J. C. I. Zebrafish heart regeneration occurs by cardiomyocyte dedifferentiation and proliferation. *Nature* **464**, 606–609 (2010).
13. Kikuchi, K., Holdway, J. E., Werdich, A. A., Anderson, R. M., Fang, Y., Egnaczyk, G. F., Evans, T., MacRae, C. A., Stainier, D. Y. R. & Poss, K. D.

1069 Primary contribution to zebrafish heart regeneration by gata4+
1070 cardiomyocytes. *Nature* **464**, 601–605 (2010).
1071 14. González-rosa, J. M., Martín, V., Peralta, M., Torres, M. & Mercader, N.
1072 Extensive scar formation and regression during heart regeneration after
1073 cryoinjury in zebrafish. **1674**, 1663–1674 (2011).
1074 15. Aurora, A. B., Porrello, E. R., Tan, W., Mahmoud, A. I., Hill, J. A., Bassel-duby,
1075 R., Sadek, H. A. & Olson, E. N. Macrophages are required for neonatal heart
1076 regeneration. **124**, (2014).
1077 16. Godwin, J. W., Debuque, R., Salimova, E. & Rosenthal, N. A. Heart
1078 regeneration in the salamander relies on macrophage-mediated control of
1079 fibroblast activation and the extracellular landscape. *npj Regen. Med.* **2**, 22
1080 (2017).
1081 17. Lai, S.-L., Marín-Juez, R., Moura, P. L., Kuenne, C., Lai, J. K. H., Tsedeke, A.
1082 T., Guenther, S., Looso, M. & Stainier, D. Y. Reciprocal analyses in zebrafish
1083 and medaka reveal that harnessing the immune response promotes cardiac
1084 regeneration. *Elife* **6**, (2017).
1085 18. Tsarouchas, T. M., Wehner, D., Cavone, L., Munir, T., Keatinge, M.,
1086 Lambertus, M., Underhill, A., Barrett, T., Kassapis, E., Ogryzko, N., Feng, Y.,
1087 van Ham, T. J., Becker, T. & Becker, C. G. Dynamic control of proinflammatory
1088 cytokines Il-1β and Tnf-α by macrophages in zebrafish spinal cord
1089 regeneration. *Nat. Commun.* **9**, 4670 (2018).
1090 19. Carrillo, S. A., Anguita-Salinas, C., Peña, O. A., Morales, R. A., Muñoz-
1091 Sánchez, S., Muñoz-Montecinos, C., Paredes-Zúñiga, S., Tapia, K. & Allende,
1092 M. L. Macrophage Recruitment Contributes to Regeneration of
1093 Mechanosensory Hair Cells in the Zebrafish Lateral Line. *J. Cell. Biochem.*
1094 **117**, 1880–1889 (2016).
1095 20. Puranik, A. S., Leaf, I. A., Jensen, M. A., Hedayat, A. F., Saad, A., Kim, K.-W.,
1096 Saadalla, A. M., Woollard, J. R., Kashyap, S., Textor, S. C., Grande, J. P.,
1097 Lerman, A., Simari, R. D., Randolph, G. J., Duffield, J. S. & Lerman, L. O.
1098 Kidney-resident macrophages promote a proangiogenic environment in the
1099 normal and chronically ischemic mouse kidney. *Sci. Rep.* **8**, 13948 (2018).
1100 21. Gurevich, D. B., Severn, C. E., Twomey, C., Greenhough, A., Cash, J., Toye,
1101 A. M., Mellor, H. & Martin, P. Live imaging of wound angiogenesis reveals
1102 macrophage orchestrated vessel sprouting and regression. *EMBO J.* **37**,

e97786 (2018).

22. Herzog, C., Pons Garcia, L., Keatinge, M., Greenald, D., Moritz, C., Peri, F. & Herrgen, L. Rapid clearance of cellular debris by microglia limits secondary neuronal cell death after brain injury in vivo. *Development* **146**, dev174698 (2019).

23. Nahrendorf, M., Swirski, F. K., Aikawa, E., Stangenberg, L., Wurdinger, T., Figueiredo, J.-L., Libby, P., Weissleder, R. & Pittet, M. J. The healing myocardium sequentially mobilizes two monocyte subsets with divergent and complementary functions. *J. Exp. Med.* **204**, 3037–3047 (2007).

24. Sager, H. B., Hulsmans, M., Lavine, K. J., Moreira, M. B., Heidt, T., Courties, G., Sun, Y., Iwamoto, Y., Tricot, B., Khan, O. F., Dahlman, J. E., Borodovsky, A., Fitzgerald, K., Anderson, D. G., Weissleder, R., Libby, P., Swirski, F. K. & Nahrendorf, M. Proliferation and Recruitment Contribute to Myocardial Macrophage Expansion in Chronic Heart Failure. *Circ. Res.* **119**, 853–64 (2016).

25. Panizzi, P., Swirski, F. K., Figueiredo, J. L., Waterman, P., Sosnovik, D. E., Aikawa, E., Libby, P., Pittet, M., Weissleder, R. & Nahrendorf, M. Impaired Infarct Healing in Atherosclerotic Mice With Ly-6Chi Monocytosis. *J. Am. Coll. Cardiol.* **55**, 1629–1638 (2010).

26. Nahrendorf, M. & Swirski, F. K. Monocyte and Macrophage Heterogeneity in the Heart. **02114**, 1624–1634 (2013).

27. Lavin, Y., Winter, D., Blecher-Gonen, R., David, E., Keren-Shaul, H., Merad, M., Jung, S. & Amit, I. Tissue-Resident Macrophage Enhancer Landscapes Are Shaped by the Local Microenvironment. *Cell* **159**, 1312–1326 (2014).

28. Xue, J., Schmidt, S. V, Sander, J., Draffehn, A., Krebs, W., Quester, I., Nardo, D. De, Gohel, T. D., Emde, M., Schmidleithner, L., Ganesan, H., Nino-castro, A., Mallmann, M. R., Labzin, L., Theis, H., Kraut, M., Beyer, M., Latz, E., Freeman, T. C., Ulas, T. & Schultze, J. L. Resource Transcriptome-Based Network Analysis Reveals a Spectrum Model of Human Macrophage Activation. *Immunity* **40**, 274–288 (2014).

29. Sanz-Morejón, A., García-Redondo, A. B., Reuter, H., Marques, I. J., Bates, T., Galardi-Castilla, M., Große, A., Manig, S., Langa, X., Ernst, A., Piragyte, I., Botos, M.-A., González-Rosa, J. M., Ruiz-Ortega, M., Briones, A. M., Salaices, M., Englert, C. & Mercader, N. Wilms Tumor 1b Expression Defines a Pro-

regenerative Macrophage Subtype and Is Required for Organ Regeneration in the Zebrafish. *Cell Rep.* **28**, 1296-1306.e6 (2019).

30. Nguyen-Chi, M., , B´eryl Laplace-BuilheTravnickova, J., Luz-crawford, P., Tejedor, G., Phan, Q. T., Duroux-richard, I., Levraud, J., Kissa, K., Lutfalla, G., Jorgensen, C., Djouad, F., Laplace-Builhe, B., Travnickova, J., Luz-crawford, P., Tejedor, G., Phan, Q. T., Duroux-richard, I., Levraud, J., Kissa, K., Lutfalla, G., Jorgensen, C. & Djouad, F. Identification of polarized macrophage subsets in zebrafish. *Elife* **4**, 1–14 (2015).
31. Matrone, G., Taylor, J., Wilson, K., … J. B.-I. journal of & 2013, undefined. Laser-targeted ablation of the zebrafish embryonic ventricle: a novel model of cardiac injury and repair. *Elsevier*.
32. Kaveh, A., Bruton, F. A., Buckley, C., Oremek, M. E. M., Tucker, C. S., Mullins, J. J., Taylor, J. M., Rossi, A. G. & Denvir, M. A. Live Imaging of Heart Injury in Larval Zebrafish Reveals a Multi-Stage Model of Neutrophil and Macrophage Migration. *Front. Cell Dev. Biol.* **8**, 579943 (2020).
33. Shiau, C. E., Kaufman, Z., Meireles, A. M. & Talbot, W. S. Differential Requirement for irf8 in Formation of Embryonic and Adult Macrophages in Zebrafish. *PLoS One* **10**, 1–15 (2015).
34. Bevan, L., Lim, Z. W., Venkatesh, B., Riley, P. R., Martin, P. & Richardson, R. J. Specific macrophage populations promote both cardiac scar deposition and subsequent resolution in adult zebrafish. *Cardiovasc. Res.* (2019) doi:10.1093/cvr/cvz221.
35. Pisharath, H., Rhee, J. M., Swanson, M. A., Leach, S. D. & Parsons, M. J. Targeted ablation of beta cells in the embryonic zebrafish pancreas using E. coli nitroreductase. *Mech. Dev.* **124**, 218–229 (2007).
36. Yoshimura, C., Nagasaka, A., Kurose, H. & Nakaya, M. Efferocytosis during myocardial infarction. *J. Biochem.* **168**, 1–6 (2020).
37. Chablais, F., Veit, J., Rainer, G. & Jaźwińska, A. The zebrafish heart regenerates after cryoinjury-induced myocardial infarction. *BMC Dev. Biol.* **11**, 21 (2011).
38. Taylor, J. M., Nelson, C. J., Bruton, F. A., Baghbadrani, A. K., Buckley, C., Tucker, C. S., Rossi, A. G., Mullins, J. J. & Denvir, M. A. Adaptive prospective optical gating enables day-long 3D time-lapse imaging of the beating embryonic zebrafish heart. *Nat. Commun.* **10**, 1–15 (2019).

39. Bajpai, G., Schneider, C., Wong, N., Bredemeyer, A., Hulsmans, M., Nahrendorf, M., Epelman, S., Kreisel, D., Liu, Y., Itoh, A., Shankar, T. S., Selzman, C. H., Drakos, S. G. & Lavine, K. J. The human heart contains distinct macrophage subsets with divergent origins and functions. *Nat. Med.* **24**, 1234–1245 (2018).

40. Lavine, K. J., Epelman, S., Uchida, K., Weber, K. J., Nichols, C. G., Schilling, J. D., David, M., Randolph, G. J., Mann, D. L., Lavine, K. J., Epelman, S., Uchida, K., Weber, K. J., Nichols, C. G. & Schilling, J. D. Distinct macrophage lineages contribute to disparate patterns of cardiac recovery and remodeling in the neonatal and adult heart. **113**, (2016).

41. Karra, R., Foglia, M. J., Choi, W.-Y., Belliveau, C., DeBenedittis, P. & Poss, K. D. Vegfaa instructs cardiac muscle hyperplasia in adult zebrafish. *Proc. Natl. Acad. Sci. U. S. A.* 201722594 (2018) doi:10.1073/pnas.1722594115.

42. Zentilin, L., Puligadda, U., Lionetti, V., Zacchigna, S., Collesi, C., Pattarini, L., Ruozi, G., Camporesi, S., Sinagra, G., Pepe, M., Recchia, F. A. & Giacca, M. Cardiomyocyte VEGFR-1 activation by VEGF-B induces compensatory hypertrophy and preserves cardiac function after myocardial infarction. *FASEB J. • Res. Commun. FASEB J* **24**, 1467–1478 (2010).

43. Kivelä, R., Hemanthakumar, K. A., Vaparanta, K., Robciuc, M., Izumiya, Y., Kidoya, H., Takakura, N., Peng, X., Sawyer, D. B., Elenius, K., Walsh, K. & Alitalo, K. Endothelial Cells Regulate Physiological Cardiomyocyte Growth via VEGFR2-Mediated Paracrine Signaling. *Circulation* **139**, 2570–2584 (2019).

44. Chimote, G., Sreenivasan, J., Pawar, N., Subramanian, J., Sivaramakrishnan, H. & Sharma, S. Comparison of effects of anti-angiogenic agents in the zebrafish efficacy-toxicity model for translational anti-angiogenic drug discovery. *Drug Des. Devel. Ther.* **8**, 1107–1123 (2014).

45. Kugler, E. C., Lessen, M., Daetwyler, S., Chhabria, K., Savage, A. M., Silva, V., Plant, K., MacDonald, R. B., Huisken, J., Wilkinson, R. N., Schulte-Merker, S., Armitage, P. & Chico, T. J. Cerebrovascular endothelial cells form transient Notch-dependent cystic structures in zebrafish. *EMBO Rep.* **20**, (2019).

46. Zhao, L., Borikova, A. L., Ben-Yair, R., Guner-Ataman, B., MacRae, C. A., Lee, R. T., Geoffrey Burns, C. & Burns, C. E. Notch signaling regulates cardiomyocyte proliferation during zebrafish heart regeneration. *Proc. Natl. Acad. Sci. U. S. A.* **111**, 1403–1408 (2014).

47. Raya, A., Koth, C. M., Büscher, D., Kawakami, Y., Itoh, T., Raya, R. M., Sternik, G., Tsai, H.-J., Rodríguez-Esteban, C. & Izpisúa-Belmonte, J. C. Activation of Notch signaling pathway precedes heart regeneration in zebrafish. *Proc. Natl. Acad. Sci. U. S. A.* **100 Suppl 1**, 11889–95 (2003).
48. Zhao, L., Ben-Yair, R., Burns, C. G. E. G. & Burns, C. G. E. G. Endocardial Notch Signaling Promotes Cardiomyocyte Proliferation in the Regenerating Zebrafish Heart through Wnt Pathway Antagonism. *Cell Rep.* **26**, 546-554.e5 (2019).
49. Samsa, L. A., Givens, C., Tzima, E., Stainier, D. Y. R., Qian, L. & Liu, J. Cardiac contraction activates endocardial Notch signaling to modulate chamber maturation in zebrafish. *Development* **142**, 4080–4091 (2015).
50. Gemberling, M., Karra, R., Dickson, A. L. & Poss, K. D. Nrg1 is an injury-induced cardiomyocyte mitogen for the endogenous heart regeneration program in zebrafish. 1–17 (2015) doi:10.7554/eLife.05871.
51. Bersell, K., Arab, S., Haring, B. & Kühn, B. Neuregulin1/ErbB4 Signaling Induces Cardiomyocyte Proliferation and Repair of Heart Injury. *Cell* **138**, 257–270 (2009).
52. Honkoop, H., Bakker, D. E. de, Aharonov, A., Kruse, F., Shakked, A., Nguyen, P. D., Heus, C. de, Garric, L., Muraro, M. J., Shoffner, A., Tessadori, F., Peterson, J. C., Noort, W., Bertozzi, A., Weidinger, G., Posthuma, G., Grün, D., Laarse, W. J. van der, Klumperman, J., Jaspers, R. T., Poss, K. D., Oudenaarden, A. van, Tzahor, E., Bakkers, J., de Bakker, D. E., Aharonov, A., Kruse, F., Shakked, A., Nguyen, P. D., de Heus, C., Garric, L., Muraro, M. J., Shoffner, A., Tessadori, F., Peterson, J. C., Noort, W., Bertozzi, A., Weidinger, G., Posthuma, G., Grun, D., van der Laarse, W. J., Klumperman, J., Jaspers, R. T., Poss, K. D., van Oudenaarden, A., Tzahor, E. & Bakkers, J. Single-cell analysis uncovers that metabolic reprogramming by ErbB2 signaling is essential for cardiomyocyte proliferation in the regenerating heart. *Elife* **8**, (2019).
53. Rasouli, S. J. & Stainier, D. Y. R. Regulation of cardiomyocyte behavior in zebrafish trabeculation by Neuregulin 2a signaling. *Nat. Commun.* **8**, 15281 (2017).
54. Uribe, V., Ramadass, R., Dogra, D., Rasouli, S. J., Gunawan, F., Nakajima, H., Chiba, A., Reischauer, S., Mochizuki, N. & Stainier, D. Y. R. In vivo analysis of

cardiomyocyte proliferation during trabeculation. (2018) doi:10.1242/dev.164194.

55. Dovey, H. F., John, V., Anderson, J. P., Chen, L. Z., De Saint Andrieu, P., Fang, L. Y., Freedman, S. B., Folmer, B., Goldbach, E., Holsztynska, E. J., Hu, K. L., Johnson-Wood, K. L., Kennedy, S. L., Kholodenko, D., Knops, J. E., Latimer, L. H., Lee, M., Liao, Z., Lieberburg, I. M., Motter, R. N., Mutter, L. C., Nietz, J., Quinn, K. P., Sacchi, K. L., Seubert, P. A., Shopp, G. M., Thorsett, E. D., Tung, J. S., Wu, J., Yang, S., Yin, C. T., Schenk, D. B., May, P. C., Altstiel, L. D., Bender, M. H., Boggs, L. N., Britton, T. C., Clemens, J. C., Czilli, D. L., Dieckman-McGinty, D. K., Droste, J. J., Fuson, K. S., Gitter, B. D., Hyslop, P. A., Johnstone, E. M., Li, W. Y., Little, S. P., Mabry, T. E., Miller, F. D., Ni, B., Nissen, J. S., Porter, W. J., Potts, B. D., Reel, J. K., Stephenson, D., Su, Y., Shipley, L. A., Whitesitt, C. A., Yin, T. & Audia, J. E. Functional gamma-secretase inhibitors reduce beta-amyloid peptide levels in brain. *J. Neurochem.* **76**, 173–181 (2001).

56. Micchelli, C. A., Esler, W. P., Kimberly, W. T., Jack, C., Berezovska, O., Kornilova, A., Hyman, B. T., Perrimon, N. & Wolfe, M. S. Gamma-secretase/presenilin inhibitors for Alzheimer's disease phenocopy Notch mutations in Drosophila. *FASEB J.* **17**, 79–81 (2003).

57. Geling, A., Steiner, H., Willem, M., Bally-Cuif, L. & Haass, C. A γ-secretase inhibitor blocks Notch signaling in vivo and causes a severe neurogenic phenotype in zebrafish. *EMBO Rep.* **3**, 688–694 (2002).

58. Gemberling, M., Karra, R., Dickson, A. L. & Poss, K. D. Nrg1 is an injury-induced cardiomyocyte mitogen for the endogenous heart regeneration program in zebrafish. *Elife* **4**, (2015).

59. Han, Y., Chen, A., Umansky, K.-B., Oonk, K. A., Choi, W.-Y., Dickson, A. L., Ou, J., Cigliola, V., Yifa, O., Cao, J., Tornini, V. A., Cox, B. D., Tzahor, E. & Poss, K. D. Vitamin D Stimulates Cardiomyocyte Proliferation and Controls Organ Size and Regeneration in Zebrafish. *Dev. Cell* **0**, (2019).

60. Vedula, V., Lee, J., Xu, H., Kuo, C. J., Hsiai, T. K. & Marsden, A. L. A method to quantify mechanobiologic forces during zebrafish cardiac development using 4-D light sheet imaging and computational modeling. 1–24 (2017).

61. Zuppo, D. A. & Tsang, M. Zebrafish heart regeneration: Factors that stimulate cardiomyocyte proliferation. *Semin. Cell Dev. Biol.* (2019)

doi:10.1016/J.SEMCDB.2019.09.005.

62. Lyons, D. A., Pogoda, H. M., Voas, M. G., Woods, I. G., Diamond, B., Nix, R., Arana, N., Jacobs, J. & Talbot, W. S. erbb3 and erbb2 are essential for Schwann cell migration and myelination in zebrafish. *Curr. Biol.* **15**, 513–524 (2005).

63. Priya, R., Allanki, S., Gentile, A., Mansingh, S., Uribe, V., Maischein, H. M. & Stainier, D. Y. R. Tension heterogeneity directs form and fate to pattern the myocardial wall. *Nature* **588**, 130–134 (2020).

64. Gálvez-Santisteban, M., Chen, D., Zhang, R., Serrano, R., Nguyen, C., Zhao, L., Nerb, L., Masutani, E. M., Vermot, J., Burns, C. G., Burns, C. E., del Álamo, J. C. & Chi, N. C. Hemodynamic-mediated endocardial signaling controls in vivo myocardial reprogramming. *Elife* **8**, (2019).

65. Nguyen-Chi, M., Laplace-builhé, B., Travnickova, J., Luz-crawford, P., Tejedor, G., Lutfalla, G., Kissa, K., Jorgensen, C. & Djouad, F. TNF signaling and macrophages govern fin regeneration in zebrafish larvae. *Nat. Publ. Gr.* **8**, e2979–e2979 (2017).

66. Kuil, L. E., Oosterhof, N., Ferrero, G., Mikulášová, T., Hason, M., Dekker, J., Rovira, M., van der Linde, H. C., van Strien, P. M. H., de Pater, E., Schaaf, G., Bindels, E. M. J., Wittamer, V. & van Ham, T. J. Zebrafish macrophage developmental arrest underlies depletion of microglia and reveals Csf1r-independent metaphocytes. *Elife* **9**, (2020).

67. Lin, X., Zhou, Q., Zhao, C., Lin, G., Xu, J. & Wen, Z. An Ectoderm-Derived Myeloid-like Cell Population Functions as Antigen Transporters for Langerhans Cells in Zebrafish Epidermis. *Dev. Cell* **49**, 605-617.e5 (2019).

68. Ginhoux, F., Schultze, J. L., Murray, P. J., Ochando, J. & Biswas, S. K. perspective New insights into the multidimensional concept of macrophage ontogeny , activation and function. **17**, (2016).

69. Koth, J., Wang, X., Killen, A. C., Stockdale, W. T., Potts, H. G., Jefferson, A., Bonkhofer, F., Riley, P. R., Patient, R. K., Göttgens, B. & Mommersteeg, M. T. M. Runx1 promotes scar deposition and inhibits myocardial proliferation and survival during zebrafish heart regeneration. *Development* **147**, (2020).

70. Herrgen, L., Voss, O. P. & Akerman, C. J. Calcium-Dependent Neuroepithelial Contractions Expel Damaged Cells from the Developing Brain. *Dev. Cell* **31**, 599–613 (2014).

71. Hill, R. A., Damisah, E. C., Chen, F., Kwan, A. C. & Grutzendler, J. Targeted two-photon chemical apoptotic ablation of defined cell types in vivo. *Nat. Commun.* **8**, 1–15 (2017).

72. van Amerongen, M. J., Harmsen, M. C., van Rooijen, N., Petersen, A. H. & van Luyn, M. J. A. Macrophage depletion impairs wound healing and increases left ventricular remodeling after myocardial injury in mice. *Am. J. Pathol.* **170**, 818–29 (2007).

73. Frantz, S., Hofmann, U., Fraccarollo, D., Schafer, A., Kranepuhl, S., Hagedorn, I., Nieswandt, B., Nahrendorf, M., Wagner, H., Bayer, B., Pachel, C., Schon, M. P., Kneitz, S., Bobinger, T., Weidemann, F., Ertl, G., Bauersachs, J., Schäfer, A., Kranepuhl, S., Hagedorn, I., Nieswandt, B., Nahrendorf, M., Wagner, H., Bayer, B., Pachel, C., Schön, M. P., Kneitz, S., Bobinger, T., Weidemann, F., Ertl, G., Bauersachs, J., Schafer, A., Kranepuhl, S., Hagedorn, I., Nieswandt, B., Nahrendorf, M., Wagner, H., Bayer, B., Pachel, C., Schon, M. P., Kneitz, S., Bobinger, T., Weidemann, F., Ertl, G. & Bauersachs, J. Monocytes/macrophages prevent healing defects and left ventricular thrombus formation after myocardial infarction. *FASEB J.* **27**, 871–881 (2013).

74. Leor, J., Palevski, D., Amit, U. & Konfino, T. Seminars in Cell & Developmental Biology Macrophages and regeneration : Lessons from the heart. *Semin. Cell Dev. Biol.* **58**, 26–33 (2016).

75. Beisaw, A., Kuenne, C., Günther, S., Dallmann, J., Wu, C.-C., Bentsen, M., Looso, M. & Stainier, D. AP-1 Contributes to Chromatin Accessibility to Promote Sarcomere Disassembly and Cardiomyocyte Protrusion during Zebrafish Heart Regeneration. *Circ. Res.* CIRCRESAHA.119.316167 (2020) doi:10.1161/CIRCRESAHA.119.316167.

76. Morikawa, Y., Zhang, M., Heallen, T., Leach, J., Tao, G., Xiao, Y., Bai, Y., Li, W., Willerson, J. T. & Martin, J. F. Actin cytoskeletal remodeling with protrusion formation is essential for heart regeneration in Hippo-deficient mice. *Sci. Signal.* **8**, (2015).

77. Itou, J., Oishi, I., Kawakami, H., Glass, T. J., Richter, J., Johnson, A., Lund, T. C. & Kawakami, Y. Migration of cardiomyocytes is essential for heart regeneration in zebrafish. *Dev.* **139**, 4133–4142 (2012).

78. de Preux Charles, A.-S., Bise, T., Baier, F., Marro, J. & Jaźwińska, A. Distinct

1341 effects of inflammation on preconditioning and regeneration of the adult
1342 zebrafish heart. *Open Biol.* **6**, 160102 (2016).
1343 79. Godwin, J. W., Debuque, R., Salimova, E. & Rosenthal, N. A. Heart
1344 regeneration in the salamander relies on macrophage- mediated control of fi
1345 broblast activation and the extracellular landscape. *npj Regen. Med.* 1–11
1346 (2017) doi:10.1038/s41536-017-0027-y.
1347 80. Marín-juez, R., Marass, M., Gauvrit, S., Rossi, A., Lai, S. & Materna, S. C. Fast
1348 revascularization of the injured area is essential to support zebrafish heart
1349 regeneration. **113**, (2016).
1350 81. Weinberger, M., Simões, F. C., Patient, R., Sauka-Spengler, T. & Riley, P. R.
1351 Functional Heterogeneity within the Developing Zebrafish Epicardium. *Dev.*
1352 *Cell* **0**, (2020).
1353 82. Stevens, S. M., von Gise, A., VanDusen, N., Zhou, B. & Pu, W. T. Epicardium
1354 is required for cardiac seeding by yolk sac macrophages, precursors of
1355 resident macrophages of the adult heart. *Dev. Biol.* **413**, 153–159 (2016).
1356 83. Deniset, J. F., Belke, D., Lee, W.-Y., Weber, G. F., Fedak, P. W. M. & Kubes,
1357 P. Gata6+ Pericardial Cavity Macrophages Relocate to the Injured Heart and
1358 Prevent Cardiac Fibrosis. *Immunity* **51**, 131-140.e5 (2019).
1359 84. Kimmel, C. B., Ballard, W. W., Kimmel, S. R., Ullmann, B. & Schilling, T. F.
1360 Stages of Embryonic Development of the Zebrafish. **10**, (1995).
1361 85. Huang, C. J., Tu, C. T., Hsiao, C. Der, Hsieh, F. J. & Tsai, H. J. Germ-line
1362 transmission of a myocardium-specific GFP transgene reveals critical
1363 regulatory elements in the cardiac myosin light chain 2 promoter of zebrafish.
1364 *Dev. Dyn.* **228**, 30–40 (2003).
1365 86. Yoo, S. K., Deng, Q., Cavnar, P. J., Wu, Y. I., Hahn, K. M. & Huttenlocher, A.
1366 Differential Regulation of Protrusion and Polarity by PI(3)K during Neutrophil
1367 Motility in Live Zebrafish. *Dev. Cell* **18**, 226–236 (2010).
1368 87. Ellett, F., Pase, L., Hayman, J. W., Andrianopoulos, A. & Lieschke, G. J.
1369 mpeg1 promoter transgenes direct macrophage-lineage expression in
1370 zebrafish. *Blood* **117**, e49 (2011).
1371 88. Renshaw, S. A., Loynes, C. A., Trushell, D. M. I., Elworthy, S., Ingham, P. W.
1372 & Whyte, M. K. B. A transgenic zebrafish model of neutrophilic inflammation.
1373 *Blood* **108**, 3976–3978 (2006).
1374 89. Mickoleit, M., Schmid, B., Weber, M., Fahrbach, F. O., Hombach, S.,

Reischauer, S. & Huisken, J. High-resolution reconstruction of the beating zebrafish heart. *Nat. Methods* **11**, 919–922 (2014).

90. Lin, Y.-F., Swinburne, I. & Yelon, D. Multiple influences of blood flow on cardiomyocyte hypertrophy in the embryonic zebrafish heart. *Dev. Biol.* **362**, 242–253 (2012).

91. Gray, C., Loynes, C. A., Whyte, M. K. B., Crossman, D. C., Renshaw, S. A. & Chico, T. J. A. Simultaneous intravital imaging of macrophage and neutrophil behaviour during inflammation using a novel transgenic zebrafish. 811–819 (2011) doi:10.1160/TH10-08-0525.

92. Davison, J. M., Akitake, C. M., Goll, M. G., Rhee, J. M., Gosse, N., Baier, H., Halpern, M. E., Leach, S. D. & Parsons, M. J. Transactivation from Gal4-VP16 transgenic insertions for tissue-specific cell labeling and ablation in zebrafish. *Dev. Biol.* **304**, 811–824 (2007).

93. Rottbauer, W., Saurin, A. J., Lickert, H., Shen, X., Burns, C. G., Wo, Z. G., Kemler, R., Kingston, R., Wu, C. & Fishman, M. Reptin and pontin antagonistically regulate heart growth in zebrafish embryos. *Cell* **111**, 661–672 (2002).

94. Ninov, N., Borius, M. & Stainier, D. Y. R. Different levels of Notch signaling regulate quiescence, renewal and differentiation in pancreatic endocrine progenitors. *Development* **139**, 1557–1567 (2012).

95. Chi, N. C., Shaw, R. M., De Val, S., Kang, G., Jan, L. Y., Black, B. L. & Stainier, D. Y. R. Foxn4 directly regulates tbx2b expression and atrioventricular canal formation. *Genes Dev.* **22**, 734–739 (2008).

96. Choi, J., Dong, L., Ahn, J., Dao, D., Hammerschmidt, M. & Chen, J. N. FoxH1 negatively modulates flk1 gene expression and vascular formation in zebrafish. *Dev. Biol.* **304**, 735–744 (2007).

97. Kikuchi, K., Gupta, V., Wang, J., Holdway, J. E., Wills, A. A., Fang, Y. & Poss, K. D. tcf21+ epicardial cells adopt non-myocardial fates during zebrafish heart development and regeneration. *Development* **138**, 2895–902 (2011).

98. Mickoleit, M., Schmid, B., Weber, M., Fahrbach, F. O., Hombach, S., Reischauer, S. & Huisken, J. High-resolution reconstruction of the beating zebrafish heart. *Nat. Methods* **11**, 919–922 (2014).

99. Almeida, R. G., Pan, S., Cole, K. L. H., Williamson, J. M., Early, J. J., Czopka, T., Klingseisen, A., Chan, J. R. & Lyons, D. A. Myelination of Neuronal Cell

Bodies when Myelin Supply Exceeds Axonal Demand. *Curr. Biol.* **28**, 1296-1305.e5 (2018).

100. Karlsson, J., Von Hofsten, J. & Olsson, P. E. Generating transparent zebrafish: A refined method to improve detection of gene expression during embryonic development. *Mar. Biotechnol.* **3**, 522–527 (2001).
101. Miskolci, V., Squirrell, J., Rindy, J., Vincent, W., Sauer, J. D., Gibson, A., Eliceiri, K. W. & Huttenlocher, A. Distinct inflammatory and wound healing responses to complex caudal fin injuries of larval zebrafish. *Elife* **8**, (2019).
102. Hoodless, L. J., Lucas, C. D., Duffin, R., Denvir, M. A., Haslett, C., Tucker, C. S. & Rossi, A. G. Genetic and pharmacological inhibition of CDK9 drives neutrophil apoptosis to resolve inflammation in zebrafish in vivo. *Sci. Rep.* **6**, 36980 (2016).
103. Burns, C. G. & MacRae, C. A. Purification of hearts from zebrafish embryos. *BioTechniques* vol. 40 274–282 (2006).

Figures:

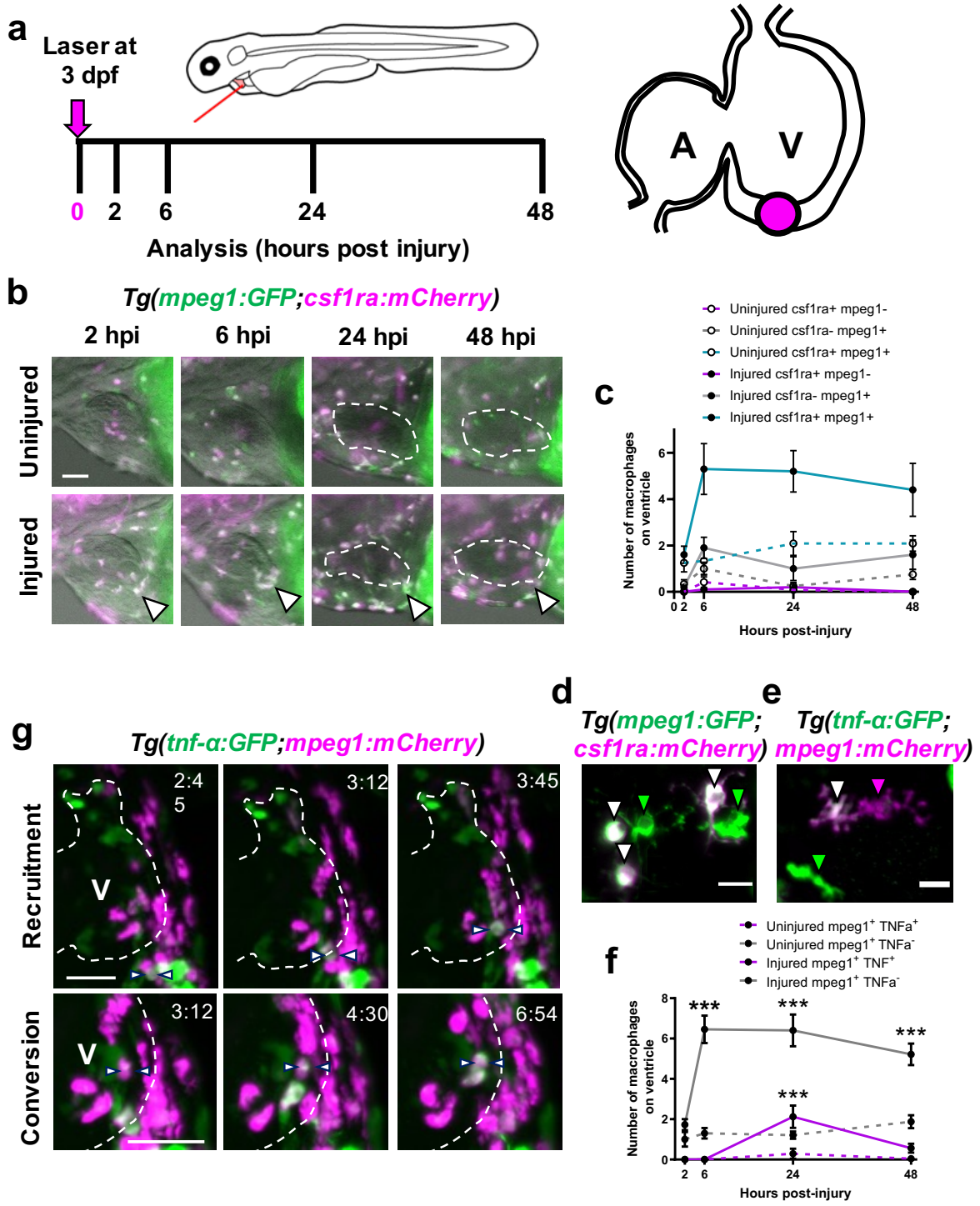

Figure 1: Cardiac macrophages display heterogeneity and plasticity following injury.

(a) Schematic illustrating the cardiac laser injury model with imaging timepoints marked (left) and the injury site at ventricular apex of a 3 dpf larval heart marked (magenta circle) (right). (b) Representative lateral view epifluorescence images of uninjured and injured hearts at the standard timepoints in *Tg(mpeg1:GFP;csf1ra:gal4;UAS:NfsB-mCherry)* (abbreviated to csf1ra:mCherry in

all panels), white arrow = ventricular apex, dashed line = heart outline. (c) Quantification of number of csf1ra+mpeg1-, csf1ra-mpeg1+ and csf1ra+mpeg1+ macrophages on the ventricle in uninjured and injured larvae at standard timepoints (n=10-12). (d) Representative epifluorescence image of csf1ra-mpeg1+ and csf1ra+mpeg1+ macrophages of different morphologies. (e) Representative epifluorescence image of tnf-*α*+mpeg1+ and tnf-*α*-mpeg1+ macrophages. (f) Quantification of number of tnf-*α*+mpeg1+ and tnf-*α*-mpeg1+ macrophages on the ventricle in uninjured and injured larvae at standard timepoints (n=10-25). (g) Time-lapse stills of injured *Tg(tnf-α:GFP;mpeg1:mCherry)* ventricles imaged live in the larvae by heart-synchronised light-sheet microscopy. Timestamps indicated, dashed line = ventricle outline, arrows = macrophage recruited as tnf-*α*+ (top) and macrophage converting to tnf-*α*+ (bottom). Scale bar = 50μm (b & g), 10μm (d & e). ****p≤0.001*, 2way ANOVA followed by Holm-Sidak's Post-hoc test.

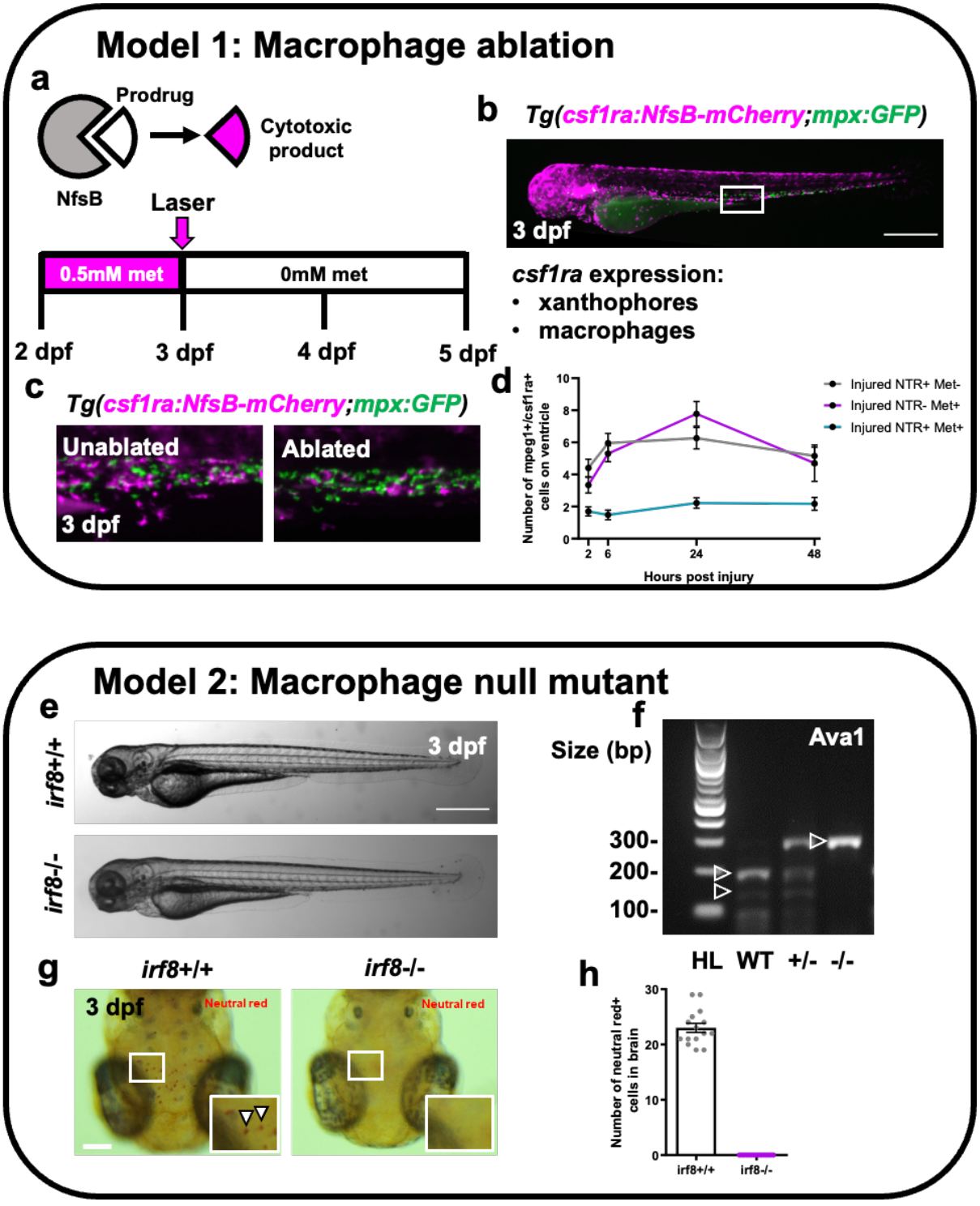

Figure 2: Macrophages can be pharmacologically ablated or developmentally blocked genetically.

(a) Schematic illustrating how nitroreductase enzyme 'NfsB' catabolises prodrug 'metronidazole' to form a cytotoxic biproduct. (b) Representative epifluorescence image of a *Tg(csf1ra:gal4;UAS:NfsB-mCherry;mpx:GFP*) 3 dpf larva (abbreviated to *Tg(csf1ra:mCherry;mpx:GFP)* in all panels), white box = caudal haematopoietic

tissue, magenta = macrophages and green = neutrophils (CHT) (c) Representative images of ablated and unablated macrophages in the CHT, size and location indicated in (b)) in *Tg(csf1ra:mCherry;mpx:GFP)* 3dpf larvae. (d) Quantification of macrophages at standard timepoints, marked by either mpeg1 or csfr1a on the injured ventricle in eavh of the NTR=metronidazole ablation model's treatment groups NTR+Met-, NTR-Met+ and NTR+Met+.(e) Representative brightfield images of *irf8+/+* and *irf8-/-* larvae at 3 dpf. (f) Representative 1% agarose gel displaying Ava1 restriction digest band pattern for WT, irf8 heterozygous and homozygous mutants. (g) Representative dorsal view brightfield image of 3 dpf larval heads stained with neutral red vital dye with white zoom panel highlighting stained macrophages (microglia) (red) in *irf8+/+* but not *irf8-/-* larvae. (h) Quantification of the number of neutral red positive stained cells (macrophages/microglia) in larval brains of *irf8+/+* and *irf8-/-* at 3 dpf. Scale bar = 500μm (b & e), 100μm (g).

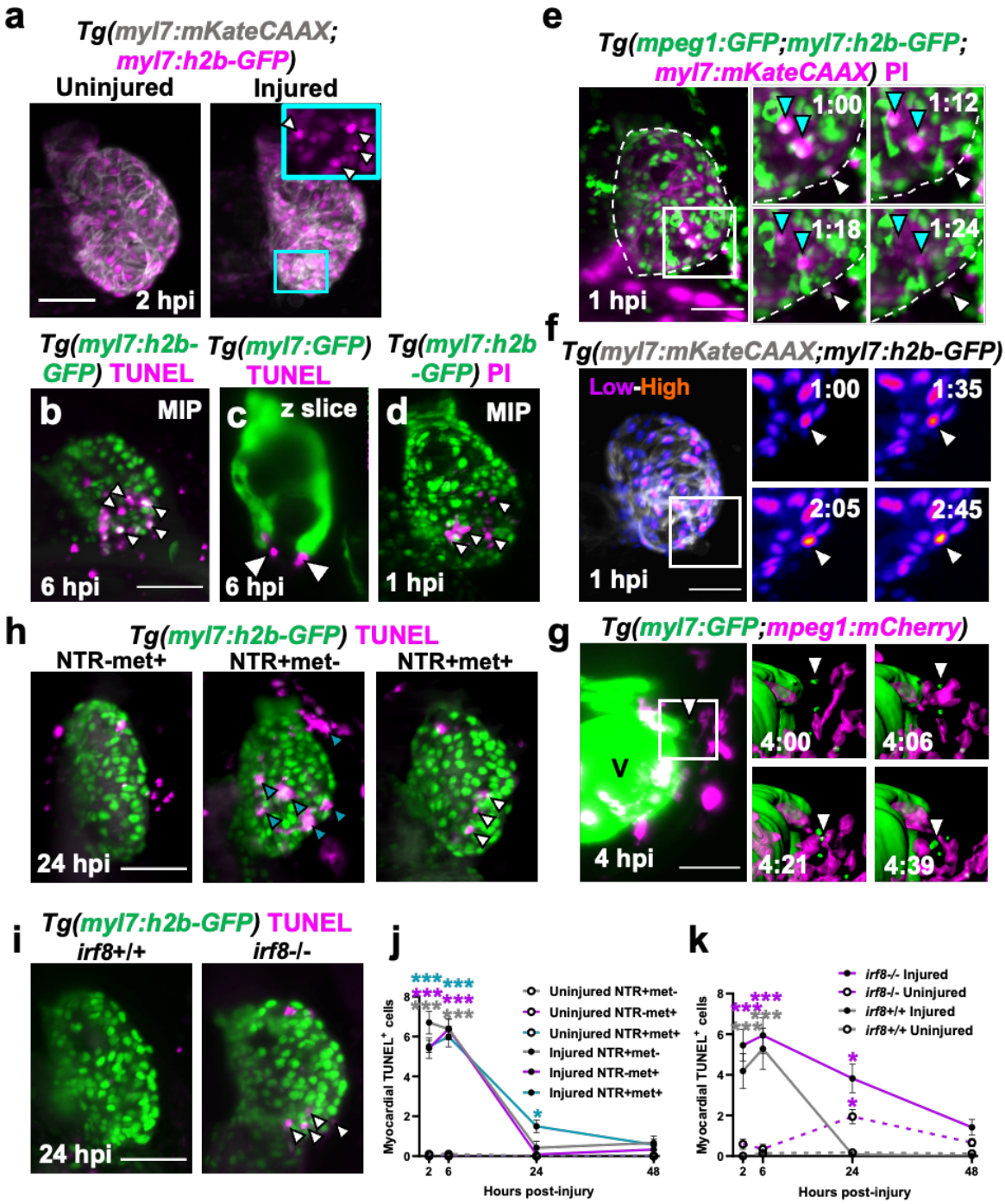

Figure 3: Macrophages are required for timely removal of apoptotic cardiomyocytes.

(a) Representative light-sheet-acquired images of uninjured and injured *Tg(myl7:h2b-GFP;myl7:mKateCAAX)* ventricles highlighting condensed nuclei in cyan outline zoom panel (white arrow-heads). (b) Representative light-sheet-acquired images of TUNEL stained hearts 6 hpi at in (b)*Tg(myl7:h2b-GFP)* and (c) *Tg(myl7:GFP)* larvae. White arrow-heads = apoptotic cardiomyocytes/myocardium.

(d) Representative light-sheet-acquired image of a propidium iodide (PI) stained *Tg(myl7:h2b-GFP)* heart 1 hpi. White arrow-heads = necrotic debris. (e) Time-lapse stills of injured *Tg(myl7:h2b-GFP;myl7:mKateCAAX;mpeg1:GFP)* ventricles imaged from 1 hpi by heart-synchronised light-sheet imaging. Round GFP^{low} = cardiomyocyte nuclei and stellate GFP^{high} =macrophages. Cyan arrow-heads = Necrotic cardiomyocyte nuclei and white arrow-heads = expelled necrotic cardiomyocyte, white box = zoom panel. (f) Time-lapse stills of injured *Tg(myl7:h2b-GFP;myl7:mKateCAAX)* ventricles imaged from 1 hpi. GFP intensity show by heat LUT, white arrow-head = apoptotic cardiomyocyte/condensing nucleus, white box = zoom panel. (g) Time-lapse stills of an injured *Tg(myl7:GFP;mpeg1:mCherry)* ventricle from 4 hpi where the full size panel has high gain in the GFP channel to highlight GFP^{low} myocardial debris and zoom panels (area indicated by white box) are surface rendered to highlight removal of myocardium (green) by macrophages (magenta). V = high gain ventricle, white arrow-head = myocardial debris. (h) Representative light-sheet acquired images of injured *Tg(myl7:h2b-GFP;csfr1a:gal4;UAS:NfsB-mCherry)* ventricles per macrophage ablation model injury group at 24 hpi. Cyan arrow-heads = Macrophages and white arrow-heads = TUNEL+ cells. (i) Representative light-sheet acquired images of *irf8+/+* and *irf8-/- Tg(myl7:h2b-GFP)* hearts stained by TUNEL at 24 hpi. White arrow-heads = TUNEL+ cells. (j) Quantification of TUNEL+ myocardial cells in uninjured and injured *Tg(myl7:h2b-GFP;csfr1a:gal4;UAS:NfsB-mCherry)* ventricles per macrophage ablation group. n=1-12 (k) Quantification of TUNEL+ myocardial cells in uninjured and injured, *irf8+/+* and *irf8-/- Tg(myl7:h2b-GFP)* ventricles. n=15-29. Scale bars = 50 μm, *$p\leq0.05$, **$p\leq0.01$, ***$p\leq0.001$ 2way ANOVA followed by Holm-Sidak's Post-hoc tests.

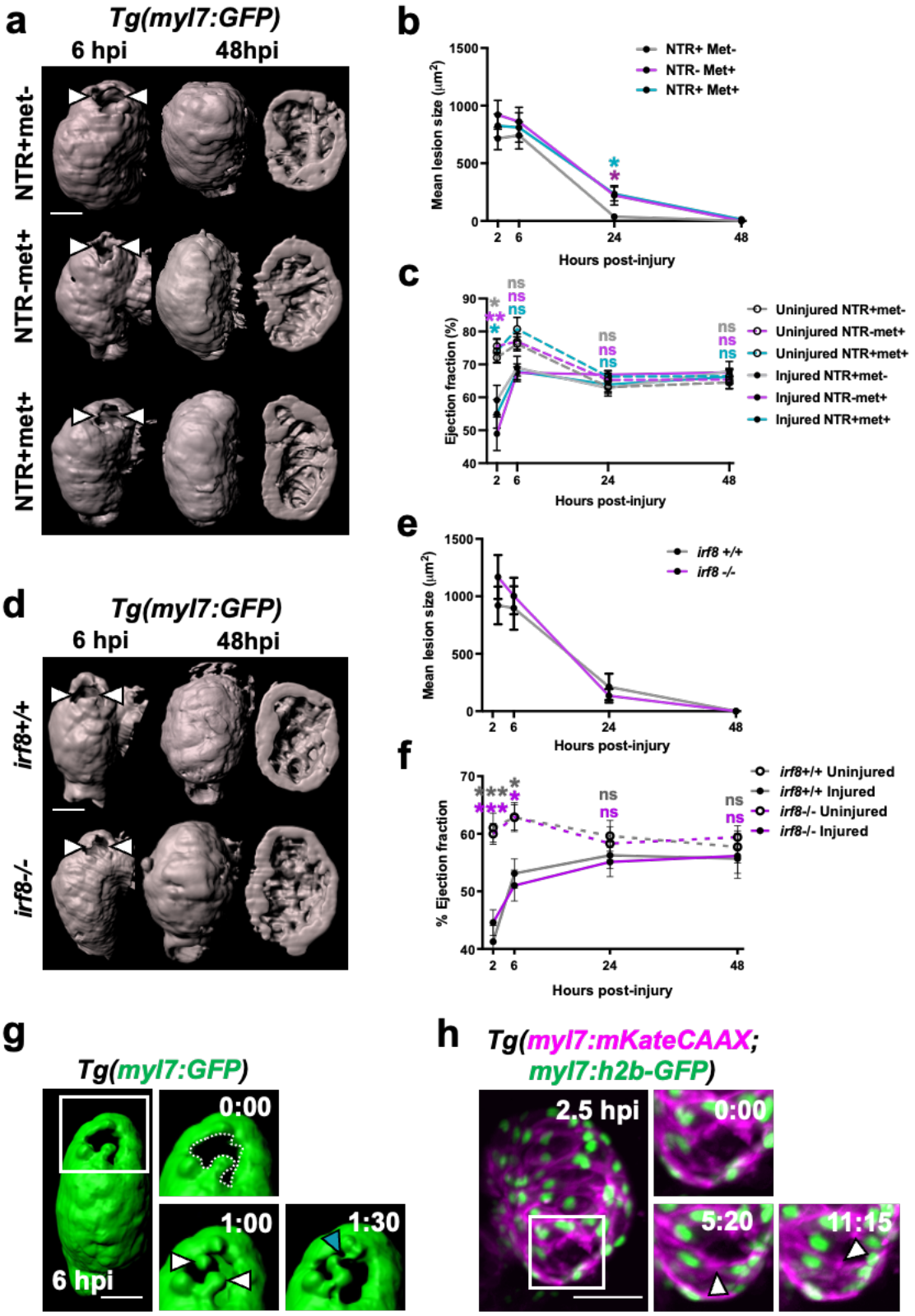

Figure 4: Macrophages not required for the recovery of cardiac structure or function.

(a) Representative GFP surface-renders of light-sheet-acquired z-stacks of injured ventricles from *Tg(myl7:GFP;csfr1a:gal4;UAS:NfsB-mCherry)* larvae, macrophage ablation groups as indicated in the figure. Abluminal myocardial surface is shown at 6 hpi (left) and abluminal and luminal surfaces shown at 48 hpi following regeneration (middle & right). White arrow-heads = laser lesion. (b) Quantification of mean lesion size in injured *Tg(myl7:GFP;csfr1a:gal4;UAS:NfsB-mCherry)* larvae per macrophage ablation group. n=11-22. (c) Quantification of ventricular ejection fraction % in uninjured and injured *Tg(myl7:GFP;csfr1a:gal4;UAS:NfsB-mCherry)* larvae per macrophage ablation group, n=10-12. (d) Representative GFP surface-renders of light-sheet-acquired z-stacks of injured ventricles from *irf8+/+* and *irf8-/- Tg(myl7:GFP)* larvae. Abluminal myocardial surface is shown at 6 hpi (left) and abluminal and luminal surfaces shown at 48 hpi following regeneration (middle & right). White arrow-heads = laser lesion. (e) Quantification of mean lesion size in injured *irf8+/+* and *irf8-/- Tg(myl7:GFP)* larvae, n=15. (f) Quantification of ventricular ejection fraction % in uninjured and injured *irf8+/+* and *irf8-/- Tg(myl7:GFP)* larvae n=15-20. (g) Time-lapse GFP-surface-rendered stills of an injured *Tg(myl7:GFP)* ventricle from 6 hpi. White box = zoom panel, white arrow-heads = myocardial buds, cyan arrow-head = myocardial bridge. (h) Time-lapse stills of an injured *Tg(myl7:mKateCAAX;myl7:h2b-GFP)* ventricle from 2.5 hpi. White box = zoom panel, white arrow-heads = cell-cell junctions *$p \leq 0.05$, ***$p \leq 0.001$ 2way ANOVA followed by Holm-Sidak's Post-hoc tests. Scale bars = 50 μm

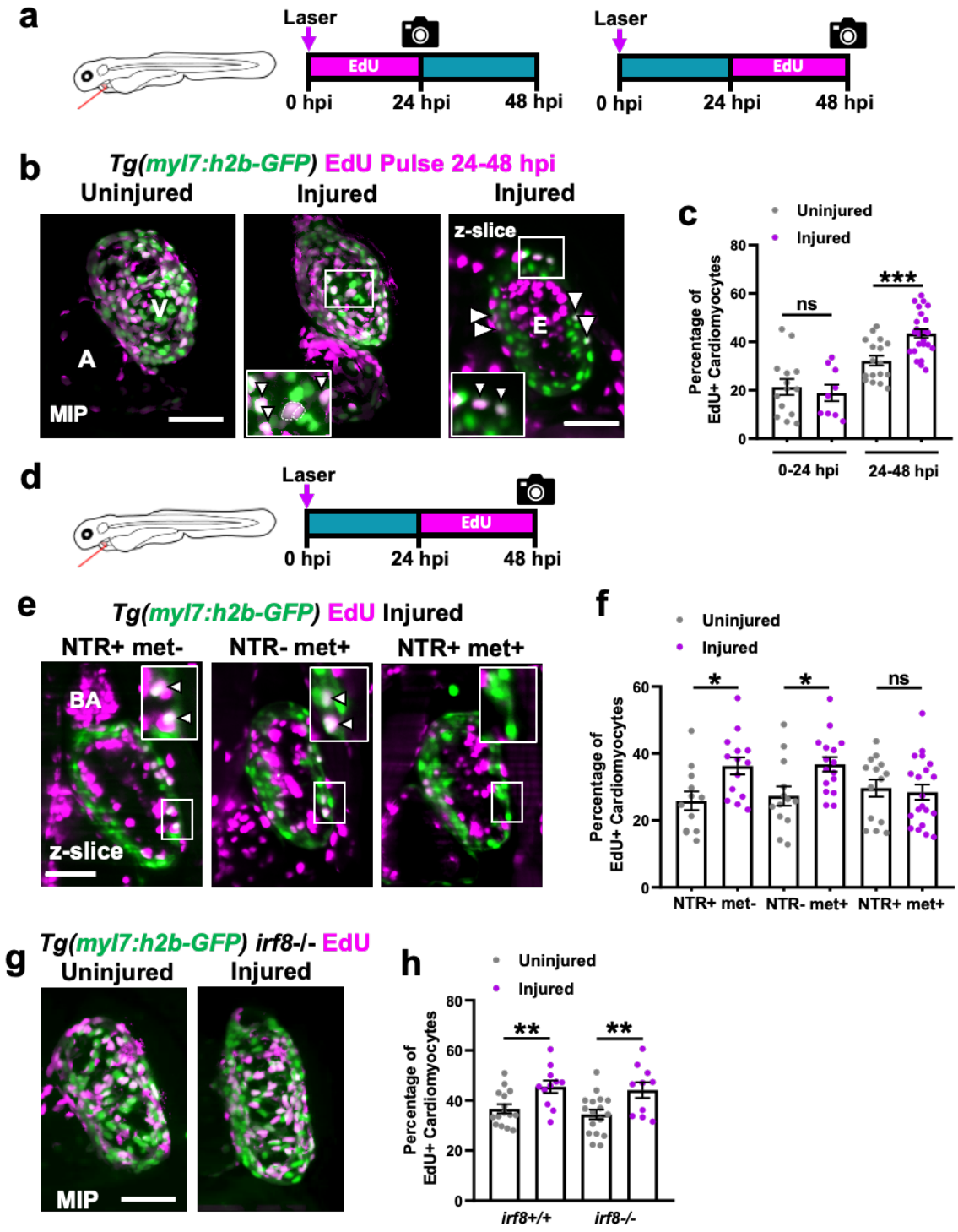

Figure 5: Macrophage ablation abolishes injury-dependent cardiomyocyte proliferation.

(a) Schematic illustrating EdU pulse strategy for labelling proliferating cardiomyocytes over 0-24 hpi (left) and 24-48 hpi (right). (b) Representative images of EdU-stained hearts from *Tg(myl7:h2b-GFP)* acquired by light-sheet microscopy at 48 hpi. Non-myocardial EdU signal is excluded post-acquistionally to allow

interpretable maximal intensity projections (MIPs). A = atrium, v = ventricle, white boxes = zoom panels, white arrow-heads = EdU+ cardiomyocyte nuclei and dashed line = outline of dividing cardiomyocyte daughter nuclei. (c) Quantification of the percentage of ventricular EdU+ cardiomyocytes in uninjured and injured *Tg(myl7:h2b-GFP)* hearts pulsed over 0-24 hpi or 24-48 hpi. ****p≤0.001* Unpaired t test. (d) Schematic illustrating EdU pulse strategy for labelling proliferating cardiomyocytes over 24-48 hpi in *Tg(myl7:h2b-GFP;csfr1a:gal4;UAS:NfsB-mCherry)* larvae per standard macrophage ablation groups. (e) Representative images of EdU-stained hearts from *Tg(myl7:h2b-GFP;csfr1a:gal4;UAS:NfsB-mCherry)* acquired by light-sheet microscopy at 48 hpi. White boxes = zoom panels, white arrow-heads = EdU+ cardiomyocyte nuclei and BA = bulbous arteriosus. (f) Quantification of the percentage of ventricular EdU+ cardiomyocytes in uninjured and injured *Tg(myl7:h2b-GFP;csfr1a:gal4;UAS:NfsB-mCherry)* hearts pulsed over 24-48 hpi. **p≤0.05* Kruskal-Wallis test and Dunn's multiple comparison Post-hoc test. (g) Representative images of uninjured and injured EdU-stained hearts from *irf8-/- Tg(myl7:h2b-GFP)* acquired by light-sheet microscopy at 48 hpi. Non-myocardial EdU signal is excluded post-acquistionally to allow interpretable maximal intensity projections (MIPs). (h) Quantification of the percentage of ventricular EdU+ cardiomyocytes in uninjured and injured *irf8+/+* and *irf8-/- Tg(myl7:h2b-GFP)* hearts pulsed 24-48 hpi. Scale bars = 50 μm. ***p≤0.01* Unpaired t test

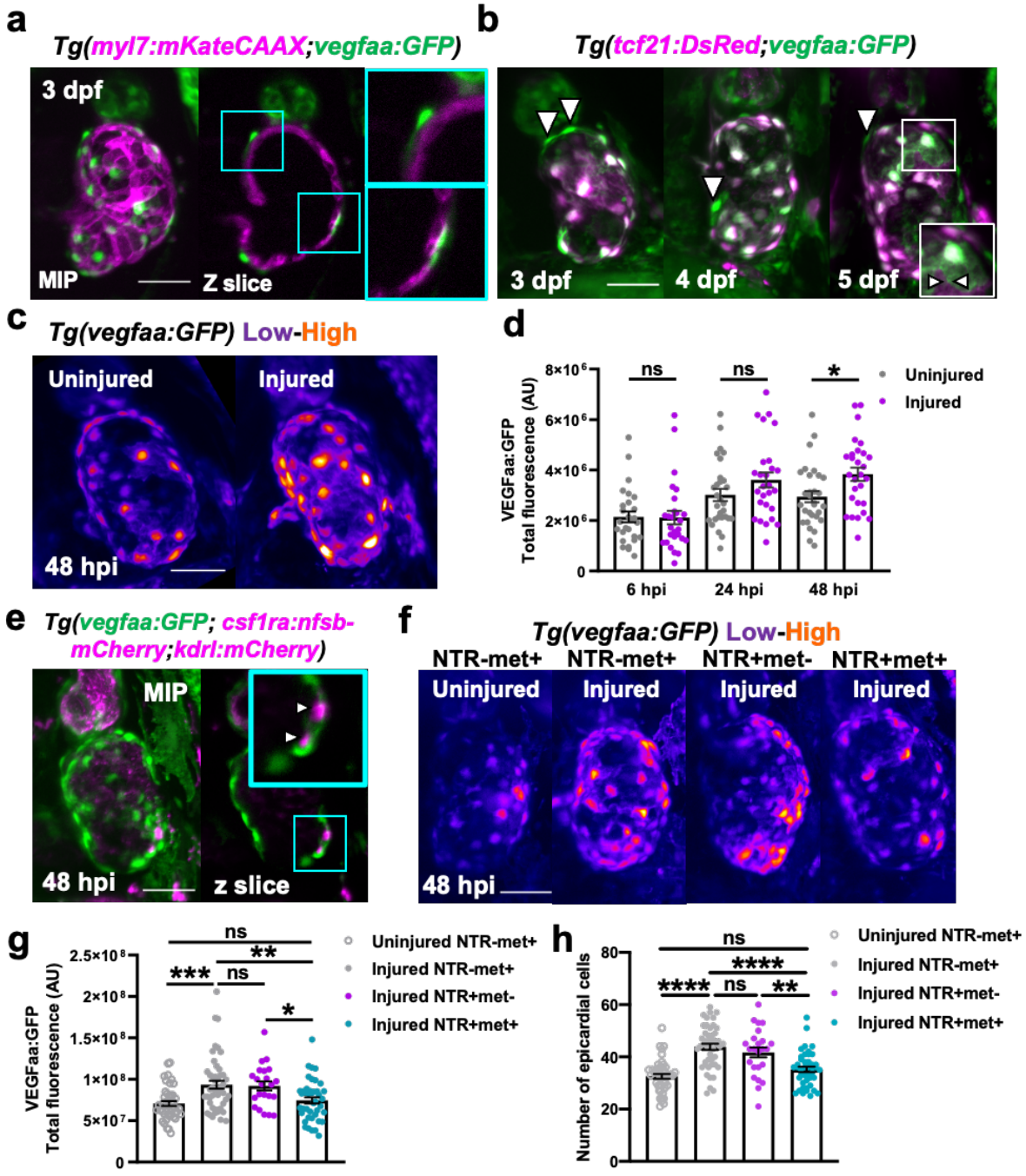

Figure 6: Macrophages stimulate epicardial expansion following cardiac injury. (a) Representative image of an uninjured 3 dpf ventricle from a *Tg(myl7:mKateCAAX;myl7:h2b-GFP)* larva acquired by light-sheet microscopy showing vegfaa+ cells (green) overlying myocardium (magenta). Cyan box = zoom panel. (b) Representative images of 3, 4 and 5 dpf ventricles from a *Tg(tcf21:DsRed;vegfaa:GFP)* larvae acquired by light-sheet microscopy showing high colocalization of vegfaa with epicardial marker tcf21. White arrow-heads =

vegfaa+tcf21- epicardial cells and white box = zoom panel. (c) Representative images of uninjured and injured ventricles from *Tg(vegfaa:GFP)* larvae acquired at 48 hpi by light-sheet microscopy. Heat LUT applied to highlight increased intensity of epicardial vegfaa:GFP in injured hearts. (d) Quantification of total ventricular VEGFaa:GFP fluorescence in uninjured and injured hearts over standard injury model timepoints, n=28-30. *$p \leq 0.05$ One way ANOVA followed by Holms-Sidak's multiple comparison Post-hoc tests. (e) Representative image of a ventricle from a *Tg(vegfaa:GFP;csfr1a:gal4;UAS:NfsB-mCherry;kdrl:hsa.HRAS-mCherry)* 48 hpi showing macrophages in the epicardial-myocardial niche (white arrow-heads). Cyan box = zoom panel. (f) Representative images of uninjured and injured ventricles from *Tg(vegfaa:GFP;csfr1a:gal4;UAS:NfsB-mCherry)* larvae from metronidazole-nitroreductase macrophage ablation groups at 48 hpi. A heat LUT is applied to highlight increase in overall fluorescence in injured groups besides NTR+met+. (g) Quantification of total vegfaa:GFP fluorescence (g) and epicardial cell number (h) in uninjured and injured ventricles from *Tg(vegfaa:GFP;csfr1a:gal4;UAS:NfsB-mCherry)* larvae from metronidazole-nitroreductase macrophage ablation groups at 48 hpi. Scale bars = 50 μm, n=46. *$p \leq 0.05$, **$p \leq 0.01$, ***$p \leq 0.001$ One way ANOVA followed by Holms-Sidak's multiple comparison Post-hoc tests.

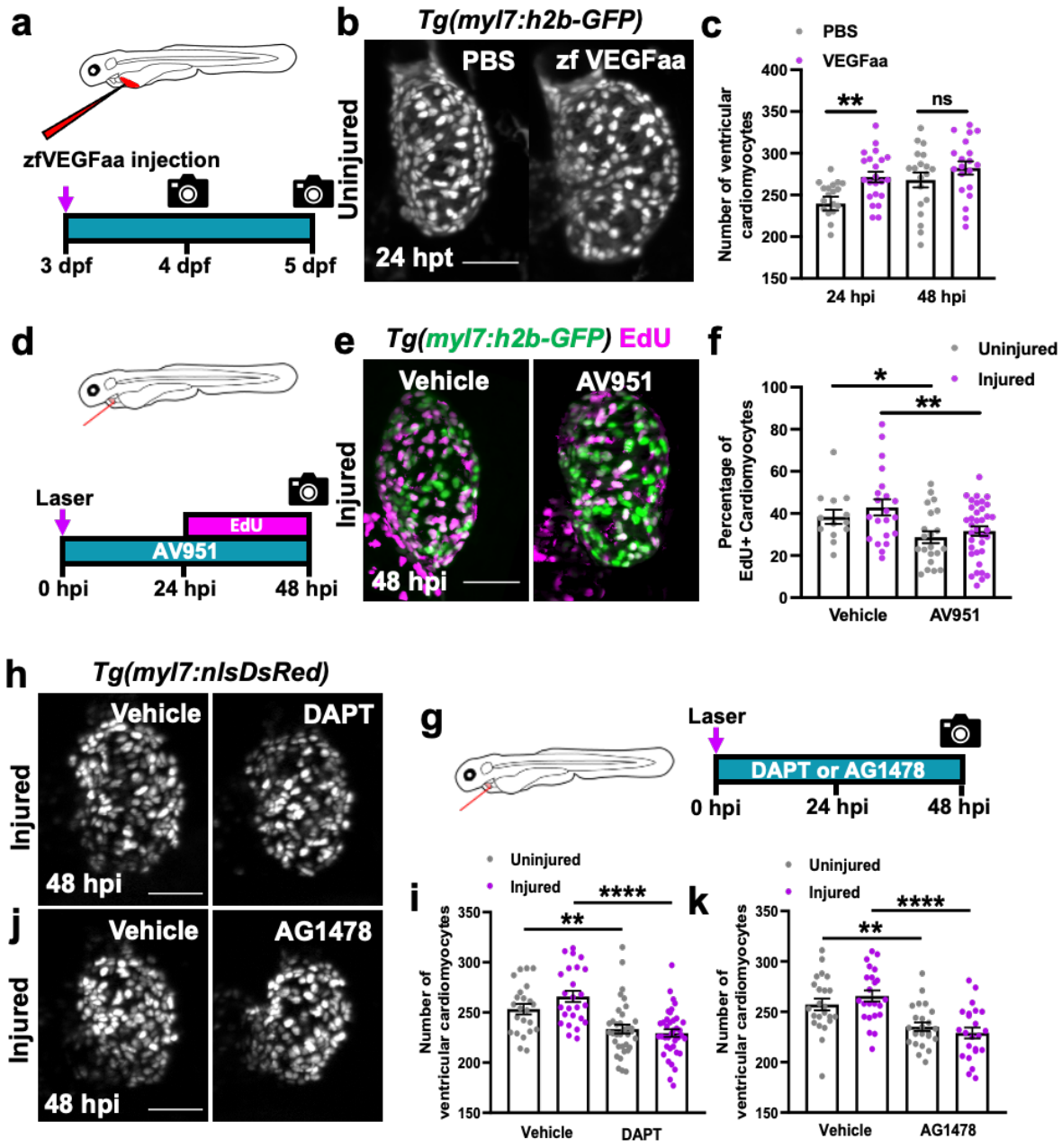

Figure 7: VEGFaa signalling is both sufficient and necessary to drive cardiomyocyte proliferation.

(a) Schematic illustrating zfVEGFaa treatment strategy via microinjection into the common cardinal vein of uninjured larvae at 72 hpi. (b) Representative light-sheet-acquired images of *Tg(myl7:h2b-GFP)* larvae at 24 hpi treated with PBS 0.1% BSA or zfVEGFaa 0.1% BSA injection. (c) Quantification of ventricular cardiomyocyte number in *Tg(myl7:h2b-GFP)* larvae at 24 and 48 hpi treated with PBS 0.1% BSA or zfVEGFaa 0.1% BSA injection, n=20. ***p≤0.01* unpaired t test. (d) Schematic illustrating AV951 treatment and EdU pulsing strategy for uninjured and injured larvae. (e) Representative images of injured ventricles from *Tg(myl7:h2b-GFP)*

larvae, EdU stained and bathed in vehicle or AV951, imaged at 48 hpi by light-sheet microscopy. Non-myocardial EdU signal is excluded post-acquistionally to allow interpretable maximal intensity projections (MIPs). (f) Quantification of the percentage of EdU+ cardiomyocyte nuclei from uninjured and injured ventricles from *Tg(myl7:h2b-GFP)* larvae, EdU stained and bathed in vehicle or AV951, n=13-36. **p≤0.05,* ***p≤0.01* unpaired t test. (g) Schematic illustrating the treatment strategy for DAPT and AV951 bathing of uninjured and injured larvae. (h) Representative images of injured *Tg(myl7:nlsDsRed)* larvae treated with vehicle or DAPT, acquired at 48 hpi by light-sheet microscopy. (i) Quantification of ventricular cardiomyocyte number in uninjured and injured *Tg(myl7:h2b-GFP)* larvae at 48 hpi treated with vehicle or DAPT, n=24-40. ***p≤0.01,* *****p≤0.0001* Unpaired t test.(j) Representative images of injured *Tg(myl7:nlsDsRed)* larvae treated with vehicle or AG1478, acquired at 48 hpi by light-sheet microscopy. (k) Quantification of ventricular cardiomyocyte number in uninjured and injured *Tg(myl7:h2b-GFP)* larvae at 48 hpi treated with vehicle or AG1478, n=24. ***p≤0.01,* *****p≤0.0001* Unpaired t test. Scale bars = 50 μm.

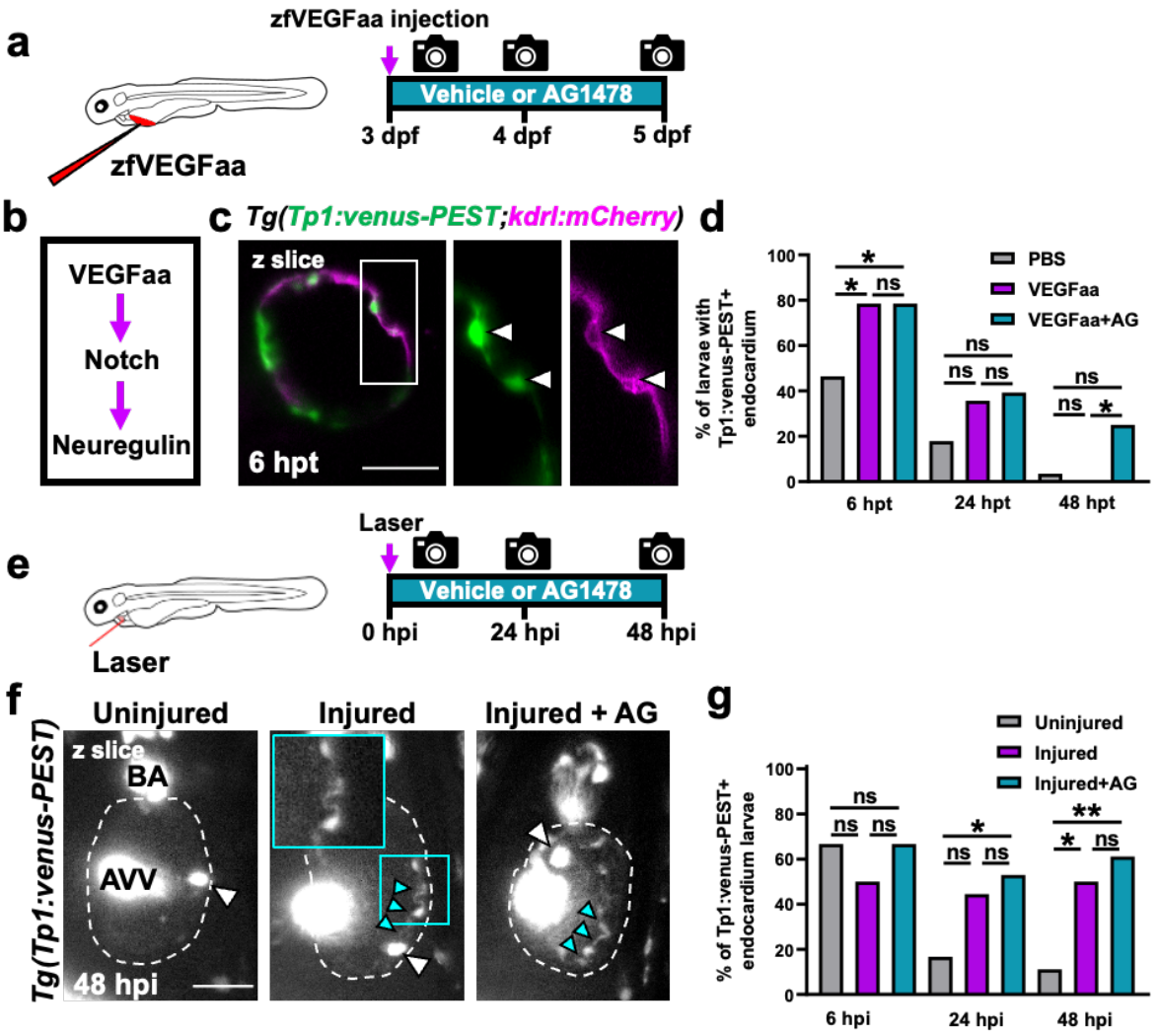

Figure 8: VEGFaa acts upstream of endocardial notch signalling.

(a) Schematic illustrating the treatment strategy for the injection of uninjured larvae with zfVEGFaa and continuous bathing in AG1478 solution. (b) Hypothesised signalling pathway active in uninjured and injured larval hearts driving cardiomyocyte proliferation. (c) Representative light-sheet-acquired z plane showing notch expression colocalising with endocardium in *Tg(Tp1:venus-PEST;kdrl:hsa.HRAS-mCherry),* abbreviated in the figure to *Tg(Tp1:venus-PEST;kdrl:has.HRAS-mCherry).* AG1478 abbreviated to AG, white box = zoom panel. (d) Quantification of the proportion of larvae with notch+ endocardium at 6, 24, and 48 hpt following zfVEGFaa injection and bathing in AG1478, n=28. *$p \leq 0.05$ Fisher's exact test. (e) Schematic illustrating the treatment strategy for the lasering of larvae and continuous bathing in AG1478 solution. (f) Representative z plane images of uninjured, injured and injured AG-treated ventricles from *Tg(tp1:venus-PEST)* larvae acquired by light-sheet microscopy at 48 hpi. BA = bulbous arteriosus, AVV = atrioventricular valve,

white arrow-heads =laterally inhibited cardiomyocytes, cyan arrow-heads = notch+ endocardium and cyan box = zoom panel. (g) Quantification of the proportion of larvae with notch+ endocardium at 6, 24, and 48 hpt following laser injury and bathing in AG1478, n=18. *$p \leq 0.05$, **$p \leq 0.01$ Fisher's exact test. Scale bars = 50 μm.

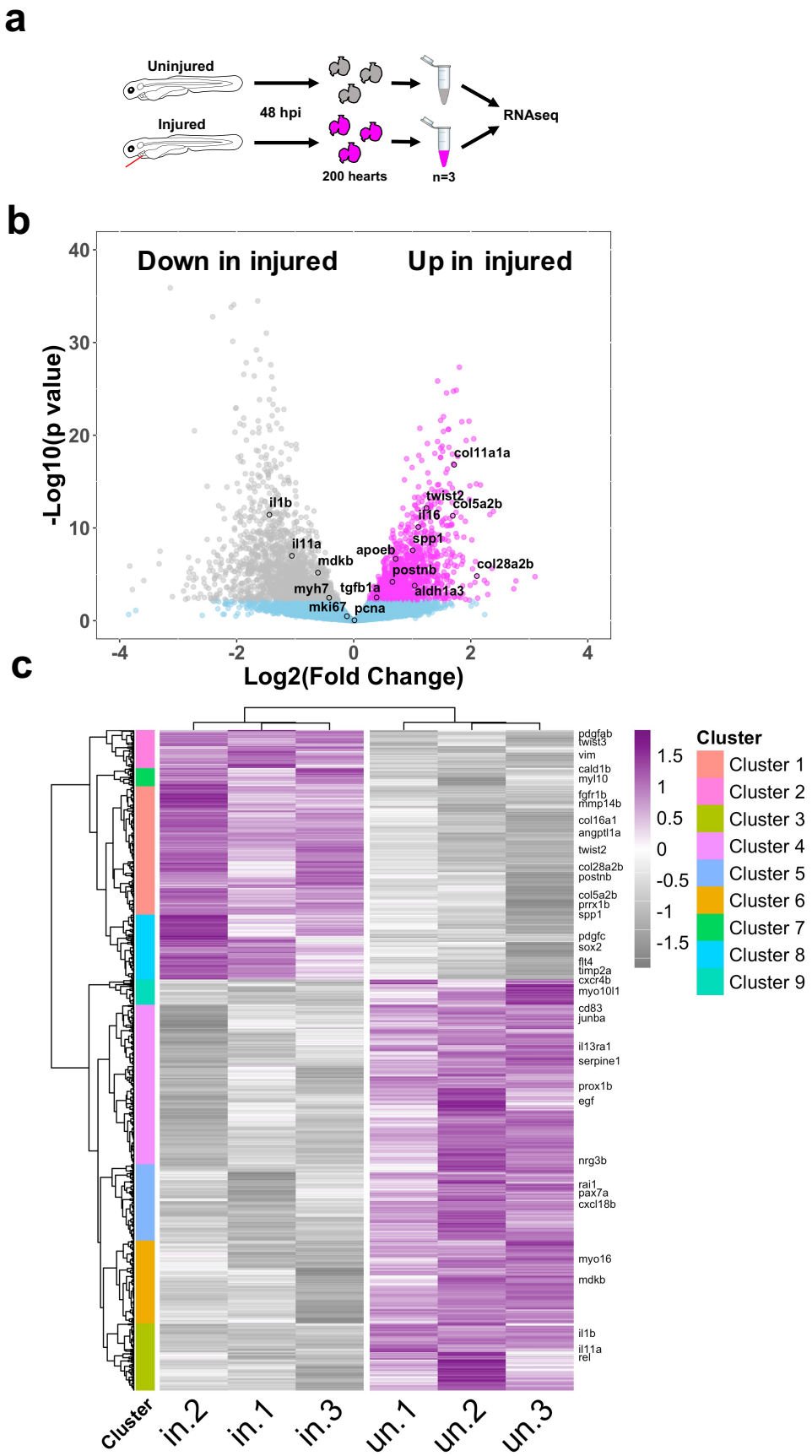

Figure 9: RNAseq analysis of larval hearts following injury

(a) Schematic illustrating the extraction of uninjured and injured hearts at 48 hpi and the pooling of 200 hearts per biological replicate for RNAseq. n=3 (b) Volcano plot showing the Log_2(Fold Change) and $–Log_{10}$(p value) for transcripts of each detected gene. Genes whose adjusted p values fall below 0.05 are deemed statistically non-significant and coloured blue. Genes up regulated in injured hearts are coloured magenta and those upregulated in uninjured hearts are coloured grey. (c) Heatmap displaying statistically significantly differentially expressed genes with a Log_2(Fold Change) >0.5. Genes were hierarchically clustered by Pearson correlation with z scaling. Clusters are indicated on the left with their dendrogram. Magenta = high expression and grey = low expression. Genes with relevance to cardiac regeneration are highlighted as annotations on the right of the plot. n=3

Supplementary figures:

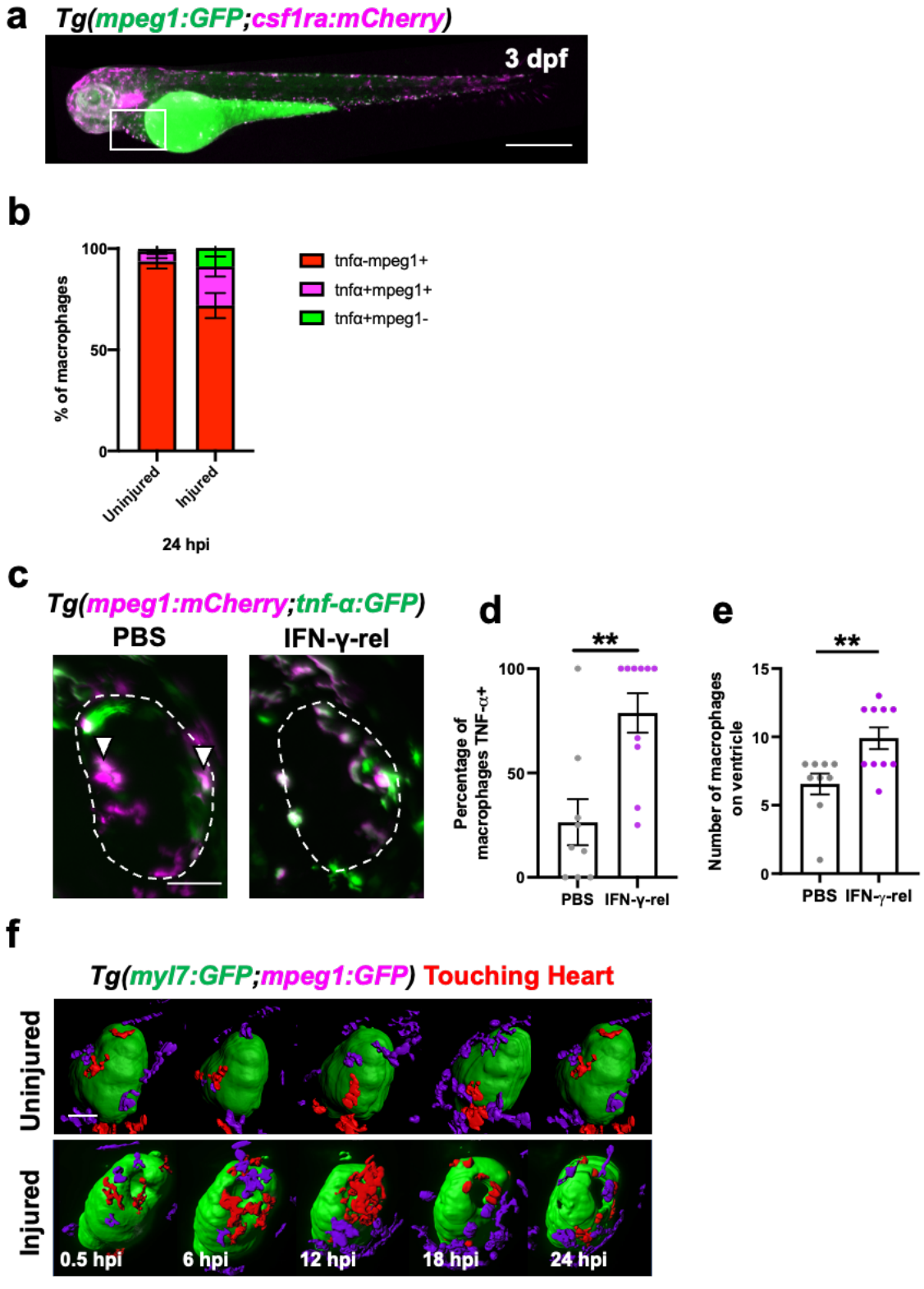

Supplementary figure 1: Cardiac macrophage phenotype in larval zebrafish is plastic and can be polarised to TNF-α+ by IFN-γ-rel.

(a) Representative epifluorescence image of a 3 dpf *Tg(mpeg1:GFP;csf1ra:gal4;UAS:NfsB-mCherry)* abbreviated to

Tg(mpeg1:GFP;csf1ra:mCherry) in the figure showing an anterior-posterior polarity in macrophage expression of csf1ra (csf1ra marking higher proportion of anterior macrophages). White box = indicated pericardial area. Scale bar = 500μm. (b) Quantification of the proportion of macrophages that are tnfα-mpeg1+, tnfα+mpeg1+ and tnfα+mpeg1- on hearts in uninured and injured larvae at 24 hpi. (c) Representative images of hearts from *Tg(mpeg1:mCherry;tnf-α:GFP)* larvae at 24 hpi injected with PBS or IFN-γ-rel. White dashed line = outline of the ventricle and white arrow-heads = tnfa+mpeg1+ macrophages. Scale bar = 50μm. (d) Quantification of the proportion of tnf-*α*+ macrophages on hearts at 24 hpi upon injection at 0 hpi with PBS or IFN-γ-rel. (e) Quantification of the number of macrophages on the injured ventricle at 24 hpi upon injection at 0 hpi with PBS or IFN-γ-rel. (f) Time-lapse stills of *Tg(myl7:GFP;mpeg1:mCherry)* hearts acquired by heart-synchronised light-sheet microscopy, surface rendered and colour coded to show myocardium in green, macrophages on the heart in red and macrophages elsewhere in purple. Macrophages can be seen to change from stellaet to rounded over time following injury. Scale bar = 50μm.

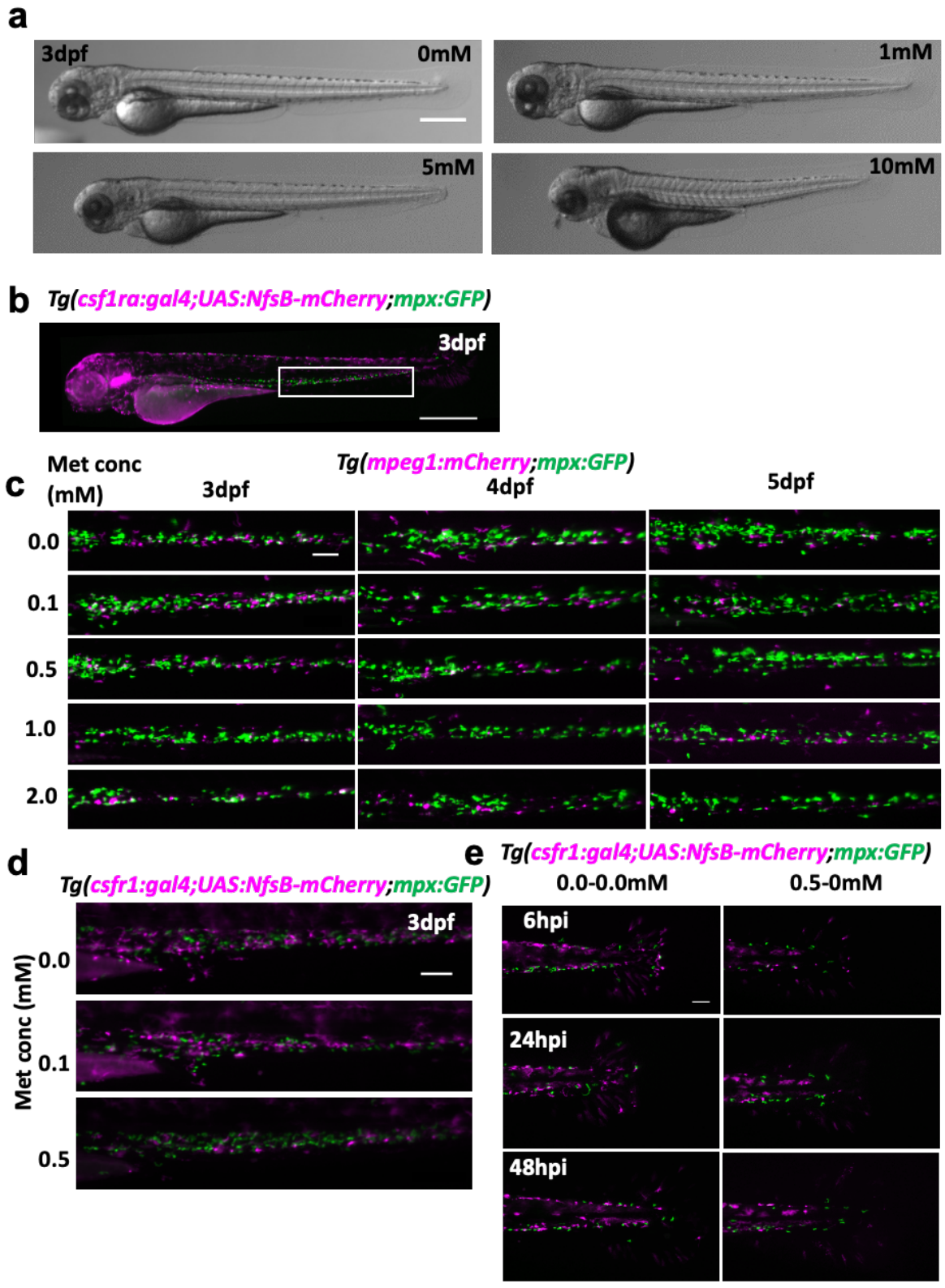

Supplementary figure 2: Optimisation of metronidazole dose for macrophage ablation.

(a) Representative brightfield images of larvae phenotype after incubation in the concentrations of metronidazole 2-3 dpf indicated in the figure. Scale bar = 500μm.

(b) Representative epifluorescence image of a 3 dpf *Tg(csf1ra:gal4;UAS:NfsB-mCherry;mpx:GFP)* larva, white box = zoom panel, scale bar = 500μm. (c) Representative epifluorescence images of CHT (region indicated by white box in (b)) at 3, 4 and 5 dpf following treatment with metronidazole (concentrations indicated in figure) 2-3 dpf. Neutrophils = green and macrophages = magenta. No NTR expression therefore toxicity to immune cells can be assessed, scale bar = 100μm (d) Representative epifluorescence images of the CHT in *Tg(csf1ra:gal4;UAS:NfsB-mCherry;mpx:GFP)* larvae incubated in the doses of metronidazole indicated in the figure 2-3 dpf. Scale bar = 100μm. (e) Representative epifluorescence images of *Tg(csf1ra:gal4;UAS:NfsB-mCherry;mpx:GFP)* tail fins resected at 72 hpi following incubation in 0.5mM metronidazole or vehicle (0mM). The macrophage response (magenta) can be seen to be blocked only in the metronidazole treated group whereas the neutrophil response is unaffected. Scale bar = 100μm.

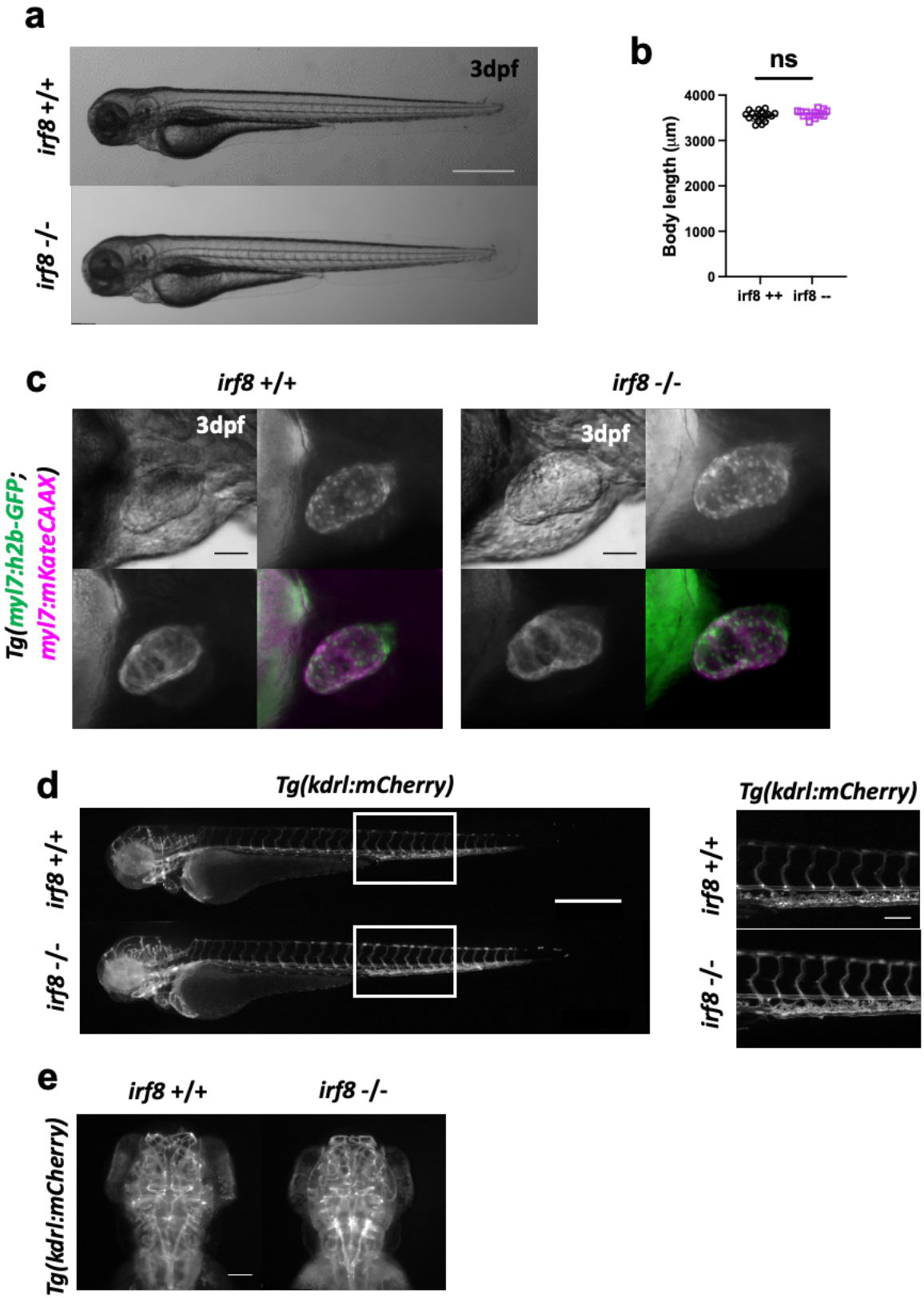

Supplementary figure 3: *irf8-/-* mutants show no overt adverse phenotype.

(a) Brightfield whole larvae image showing no morphological difference between *irf8-/-* and *irf8*+/+ at 3 dpf, scale bar = 500μm. (b) Quantification of body length in *irf8*+/+

and *irf8-/-* showing no difference between genotypes. (c) Brightfield and epifluorescence images of a laterally viewed heart from *irf8+/+ and irf8-/- Tg(myl7:h2b-GFP;myl7:mKateCAAX)* larvae at 3 dpf showing no cardiac abnormalities in *irf8-/-* larvae. Scale bar = 50μm (d) Epifluorescence whole larvae image of *irf8+/+ and irf8-/- Tg(kdrl:mCherry)* larvae showing no vascular abnormalities in *irf8-/-* larvae. Scale bar = 500μm. White boxes = zoom panels (right, scale bar = 100μm). (e) Dorsal view representative epifluorescence images of cranial vasculature in *Tg(kdrl:mCherry)* showing no difference between *irf8+/+* and *irf8-/-* larvae, scale bar = 100μm.

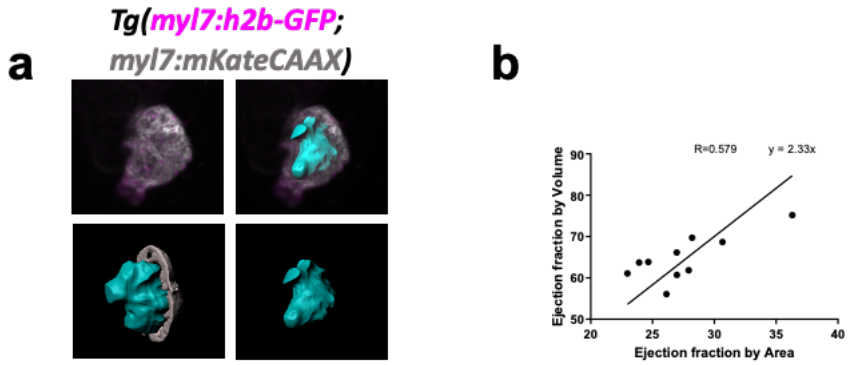

Supplementary figure 4: Ejection fraction by area is proportional to ejection fraction by volume.

(a) Representative IMARIS-generated image showing a rendered ventricular myocardium (grey render), rendered chamber volume (cyan) and MIP of 3D heart synchronised light-sheet scan of a 3 dpf heart (ventricle) in diastole. Image acquired from a *Tg(myl7:h2b-GFP;myl7:mKateCAAX)* larva. (b) Quantification of ejection fraction by area (calculated by diastolic and systolic lateral brightfield) and by volume (calculated by surface renders of luminal volumes in diastole and systole) per fish.

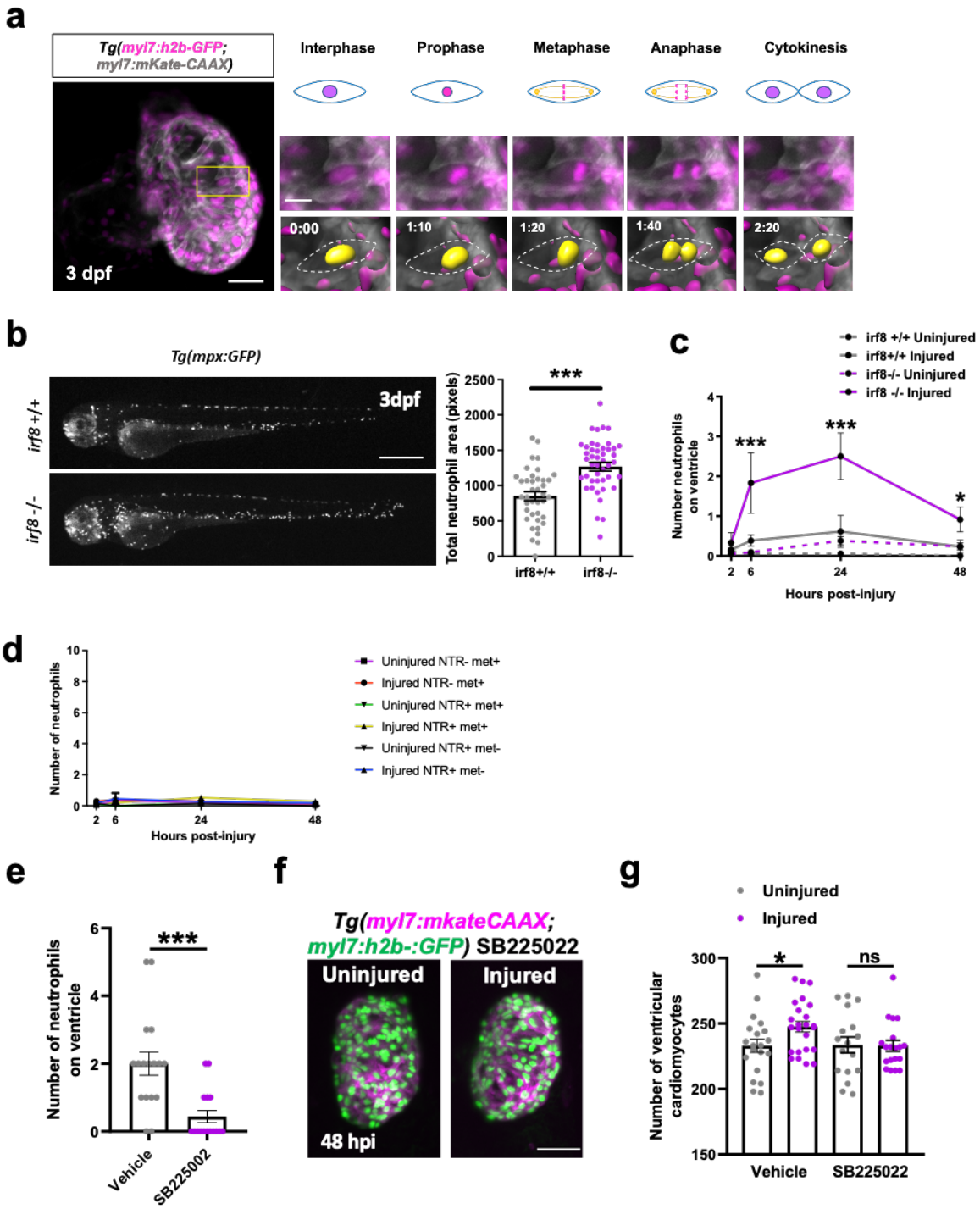

Supplementary figure 5: *irf8-/-* larvae have a larger neutrophil response to cardiac injury than *irf8+/+*.

(a) Representative stills from heart synchronised light-sheet timelapse of a laser injured 3 dpf *Tg(myl7:h2b-GFP;myl7:mKateCAAX)* larva showing an example of each phase of complete cell division of a single cardiomyocyte, typical of larval hearts. Yellow box = zoom panel, left scale bar = 30 μm and right scale bar = 10 μm. Timestamps post-injury indicated in figure. (b) Representative whole larva

epifluorescence image of *irf8-/-* and *irf8+/+ Tg(mpx:GFP)* larvae showing *irf8-/-* to have greater global neutrophil numbers (scale bar = 500 μm), quantified in the graph (right). ****p≤0.001.* t test, n=39-46. (c) Quantification of neutrophil numbers at the ventricle in uninjured and injured *irf8+/+* and *irf8-/-* larvae at the standard laser-injury model timepoints showing *irf8-/-* larvae to have a significantly greater neutrophil response, n=17-25. (d) Quantification of neutrophil numbers at the ventricle in uninjured and injured NTR-met+, NTR+met+ and NTR+met- larvae at the standard laser-injury model timepoints showing all metronidazole-nitroreductase treatment groups to have a minimal neutrophil response and therefore no neutrophil compensation in the macrophage ablated group NTR+met+, n=17-24. (e) Quantification of the number of recruited neutrophils at the injured ventricle in at 24 hpi in *Tg(myl7:h2b-GFP;myl7:mKateCAAX)* larvae bathed in vehicle or SB225002 -2 to 24 hpi showing SB225002 to significantly reduce neutrophil number, n=17. (f) Representative light-sheet acquired images of uninjured and injured *irf8-/- Tg(myl7:h2b-GFP;myl7:mKateCAAX)* ventricles at 48 hpi following treatment with SB225002 -2 to 24 hpi, scale bar = 50 μm. (g) Quantification of ventricular cardiomyocyte number in uninjured and injured *irf8-/- Tg(yl7:h2b-GFP;myl7:mKateCAAX)* ventricles at 48 hpi following treatment with vehicle or SB225002 -2 to 24 hpi, n=17-20, **p≤0.05.* t test

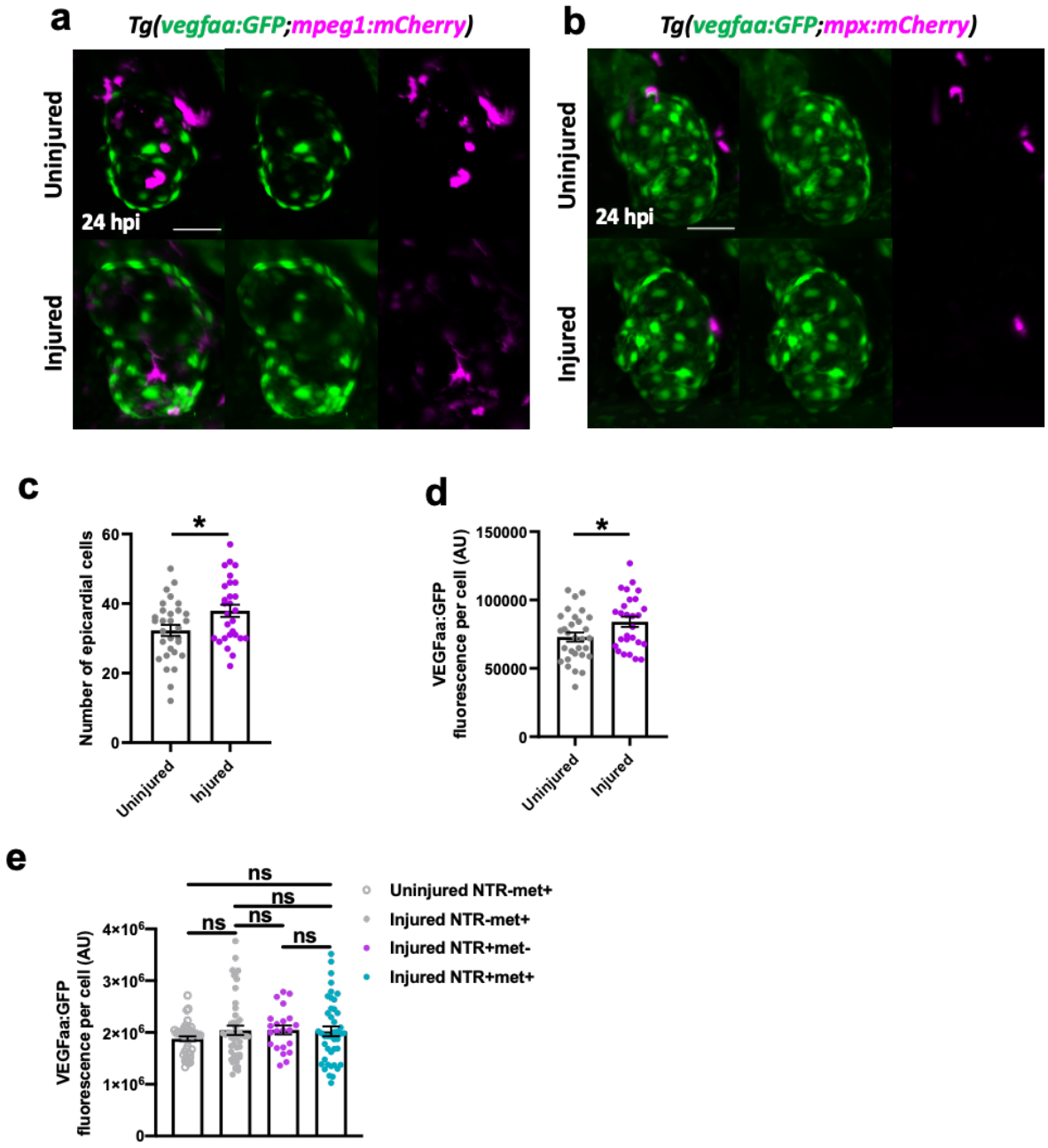

Supplementary figure 6: vegfaa:GFP expression does not colocalize with macrophages or neutrophils following larval heart injury.

(a) Representative light-sheet-acquired image of an injured *Tg(vegfaa:GFP;mpeg1:mCherry)* heart 24 hpi showing VEGFaa expression only in the epicardium and not in macrophages, scale bar = 100μm. (b) Representative light-sheet-acquired image of an injured *Tg(vegfaa:GFP;mpx:mCherry)* heart 24 hpi showing VEGFaa expression only in the epicardium and not in neutrophils, scale bar = 100μm. (c) Quantification of the number of epicardial cells, as marked by

vegfaa:GFP, on injured ventricles at 48 hpi in uninjured and injured larvae, n=30. *$p \leq 0.05$ t test (d) Quantification of the average vegfaa:GFP expression of epicardial cells per cell, on injured ventricles at 48 hpi in uninjured and injured larvae, n=30. *$p \leq 0.05$ t test (e) Quantification of average vegfaa:GFP fluorescence per cell in metronidazole-nitroreductase ablation model groups at 48 hpi, n=22-44. One-way ANOVA followed by Holm-Sidak's multiple comparisons Post-hoc test.

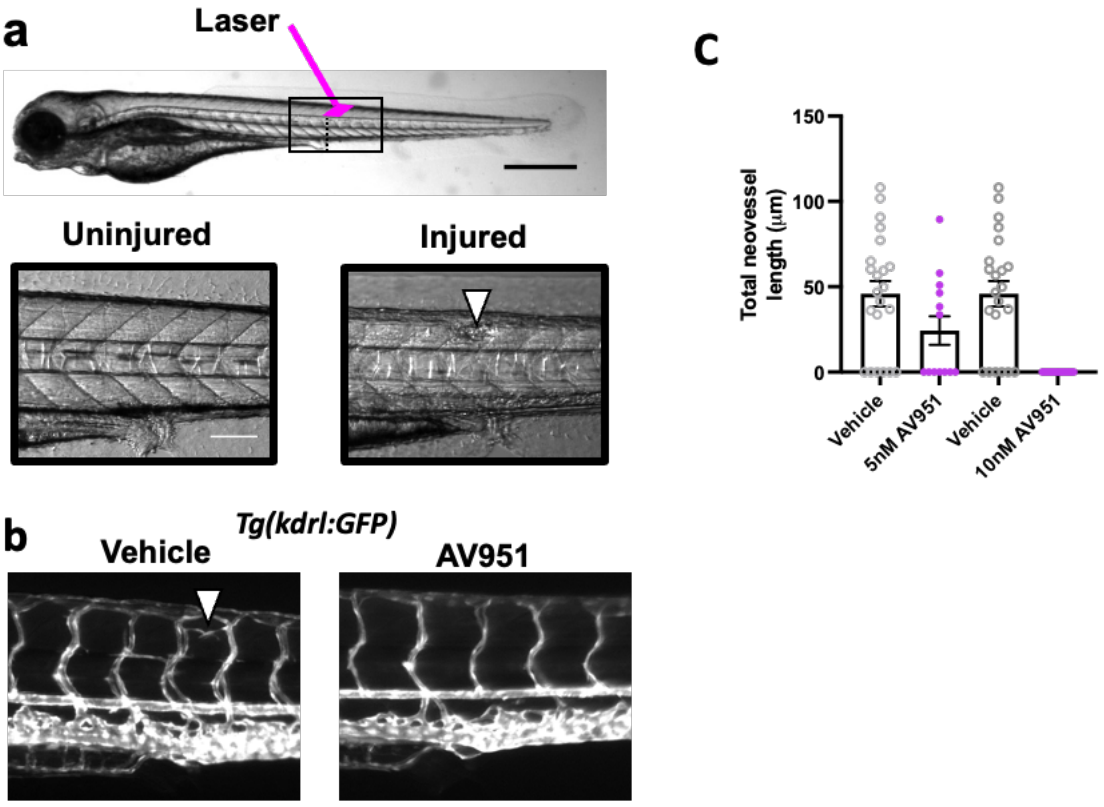

Supplementary figure 7: 10nM VEGFR pan antagonist AV951 entirely abolishes inflammatory angiogenesis.

(a) Annotated brightfield image of a 3 dpf whole larva (0 hpi) with the somite used for laser injury highlighted in magenta, scale bar = 500μm .Black box = zoom panel for lower panels. Lower panels show the laser lesion site (white arrow), scale bar = 100μm. (b) Representative epifluorescence images of trunk vasculature surrounding the laser lesioned muscle segment/somite in vehicle and 10nM AV951 treated (0-48 hpi) larvae at 48 hpi. White arrow = neovasculature. (c) Quantification of

neovasculature length at 48 hpi after laser injury for vehicle, 5 nM and 10nM AV951-treated larvae, n=13-22.

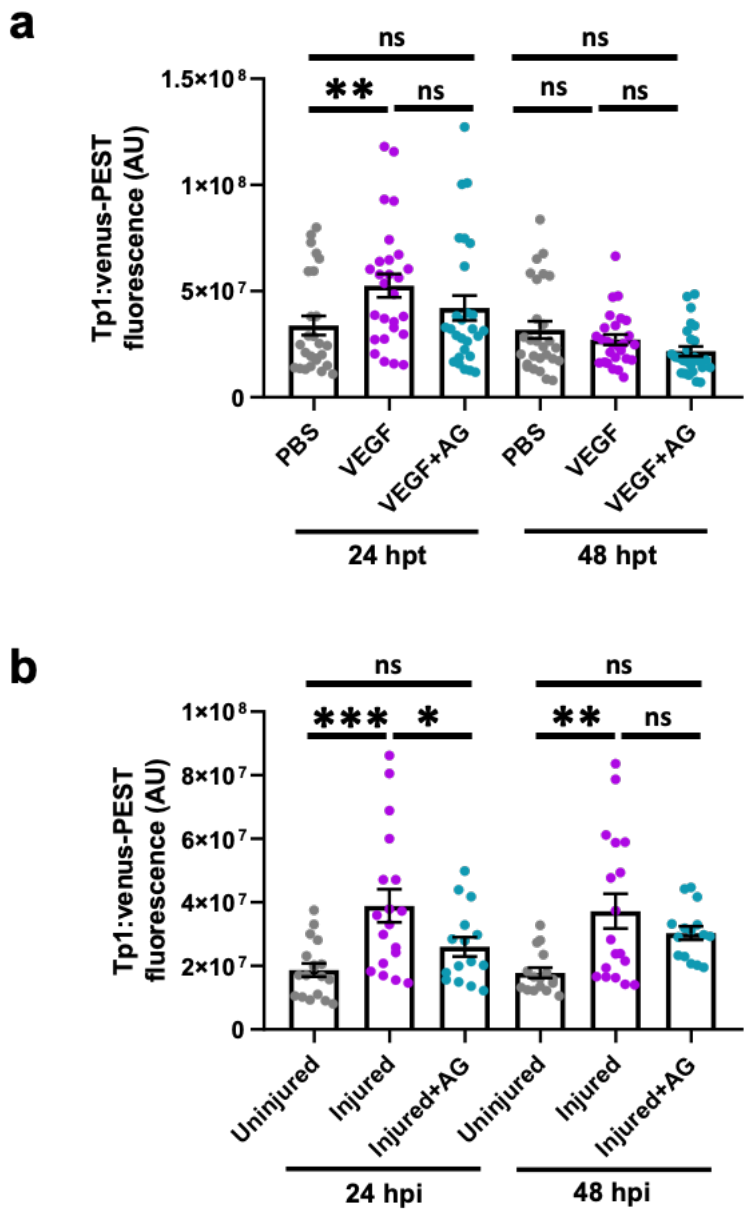

Supplementary figure 8: VEGFaa injection and injury increase myocardial notch signaling in a Nrg-ERRB dependent manner.

(a) Quantification of total ventricular myocardial from *Tg(Tp1:venus-PEST)* hearts following injection with PBS or zfVEGFaa or injection with zfVEGFaa and incubation in pan ERRB antagonist AG1478, n=28 (b) Quantification of total ventricular myocardial from *Tg(Tp1:venus-PEST)* uninjured hearts and in hearts following laser injury or laser injury and in pan ERRB antagonist AG1478, n=18. *$p \leq 0.05$, **$p \leq 0.01$,

***$p \leq 0.001$, One way ANOVA followed by Holm-Sidak's multiple comparisons Post-hoc test.

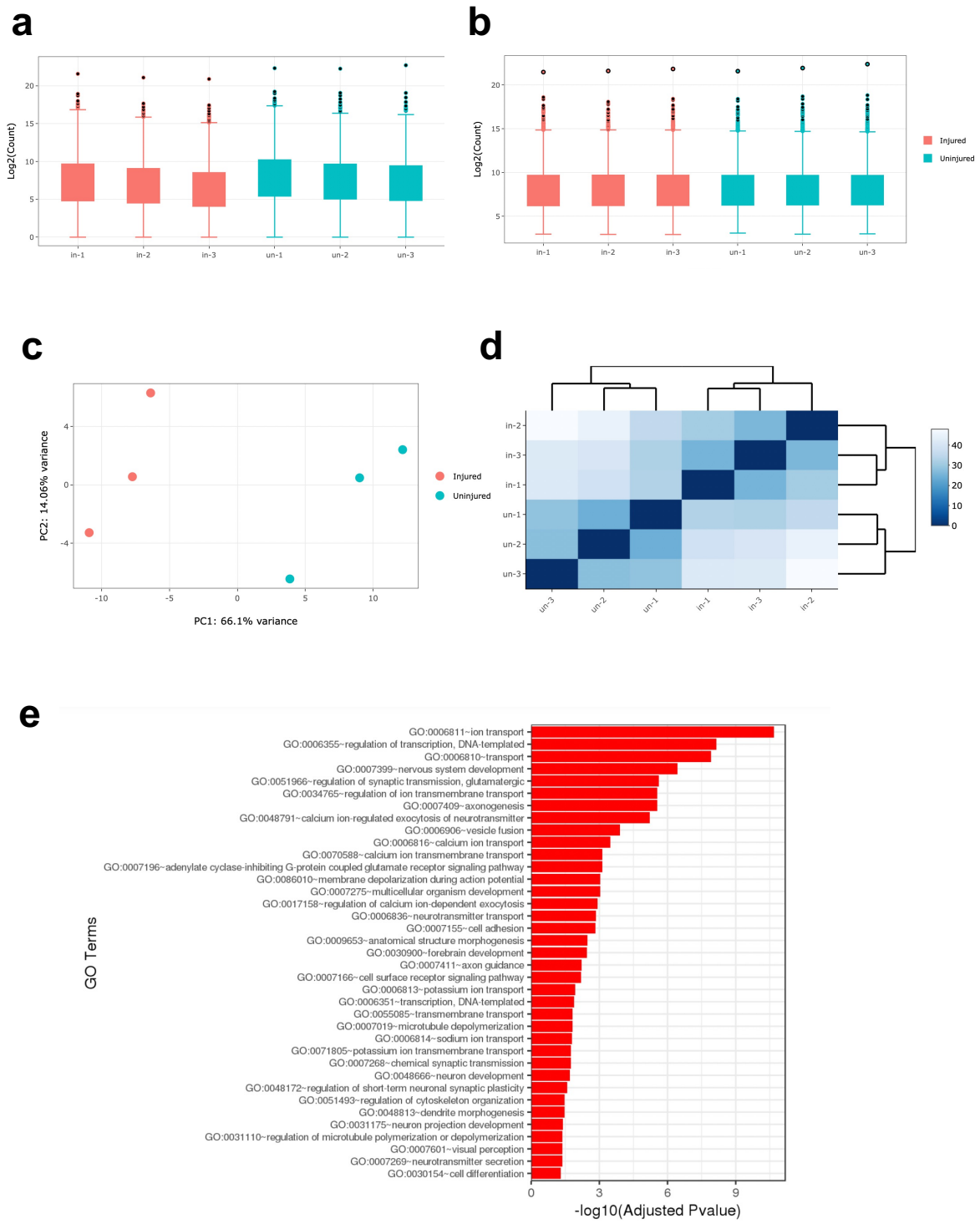

Supplementary figure 9: Bulk RNAseq analysis of uninjured and injured larval hearts

(a) Box plot illustrating the distribution of reads before (a) and after normalisation (b). (c) Principle component analysis of samples illustrating sample similarity. (d) Distance matrix illustrating pairwise sample similarity. (e) Plot showing gene ontology terms that were significantly enriched by Fishers exact test for significantly (padj<0.05) differentially expressed genes between uninjured and injured hearts at 48. hpi.

Videos:

Videos 1-8 can be found deposited on Dropbox via the following link: https://www.dropbox.com/s/h91m523wiab6kh0/Videos.zip?dl=0

Video 1: LSFM-acquired heartbeat-synchronised timelapse of a *Tg(csf1ra:mCherry;mpeg1:GFP)* heart showing macrophage heterogeneity following cardiac injury.

Video 2: LSFM-acquired heartbeat-synchronised timelapse of a *Tg(mpeg1:mCherry;tnfa:GFP)* heart showing macrophage plasticity following cardiac injury.

Video 3: LSFM-acquired heartbeat-synchronised timelapse of a *Tg(myl7:h2b-GFP;mpeg1:GFP)* heart injected with propdium iodide showing PI+ cardiomyocyte expulsion following cardiac injury.

Video 4: LSFM-acquired heartbeat-synchronised timelapse of a *Tg(myl7:h2b-GFP;myl7:mKateCAAX)* heart following cardiac injury showing cardiomyocyte apoptosis following injury.

Video 5: LSFM-acquired heartbeat-synchronised timelapse of a *Tg(myl7:GFP;mpeg1:mCherry)* heart, 3D surface rendered, showing removal and internalization of myocardial debris by macrophages following injury.

Video 6: LSFM-acquired heartbeat-synchronised timelapse of a *Tg(myl7:GFP)* heart, 3D surface rendered, showing budding and bridging of wound margin myocardium following injury.

Video 7: LSFM-acquired heartbeat-synchronised timelapse of a *Tg(myl7:h2b-GFP;myl7:mKateCAAX)* heart, showing budding and bridging of individual wound-margin cardiomyocytes following injury.

Video 8: LSFM-acquired heartbeat-synchronised timelapse of a *Tg(myl7:h2b-GFP;myl7:mKateCAAX)* heart, showing cardiomyocyte cell division with nuclear division and cytokinesis.